

Further Approaches in the Design of Antitumor Agents with Response to Cell Resistance: Looking toward Aza Crown Ether-dtc Complexes

Antonino Arenaza-Corona, M. Delfina Couce-Fortúnez, Andrés de Blas, David Morales-Morales, Rosa Santillan, Herbert Höpfl, Teresa Rodríguez-Blas,* and Victor Barba*

Cite This: <https://dx.doi.org/10.1021/acs.inorgchem.0c02068>

Read Online

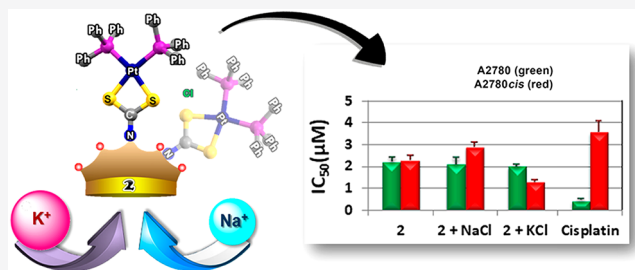
ACCESS |

Metrics & More

Article Recommendations

Supporting Information

ABSTRACT: The dianionic aza crown ether-dtc N,N' -bis-(dithiocarbamate)-1,10-diaza-18-crown-6 (L^{2-}) is a versatile ligand capable of yielding binuclear complexes with group 10 elements, also known as Ni-triade, $[\mu-(\kappa^2-S,S'-L)M_2(PPh_3)_4]Cl_2$ ($M = Pd$ (1), Pt (2)), $[\mu-(\kappa^2-S,S'-L)M_2(PPh_3)_4](BPh_4)_2$ ($M = Pd$ (3), Pt (4)), and $\mu-(\kappa-S,S'-L)Ni_2(PPh_3)_2Cl_2$ (5), and has proven to be an excellent option to the design of metal-based drugs able to provide multiple response to cell resistance. Palladium and platinum complexes, 1 and 2, were tested for cytotoxicity in the human cervix carcinoma cell line HeLa-229, the human ovarian carcinoma cell line A2780, and the cisplatin-resistant mutant A2780cis, finding significant activity toward all three cancer cell lines, with low micromolar IC_{50} values, comparable to cisplatin. Markedly, against the cisplatin resistant cell line A2780cis, compound 2 exhibits better cytotoxic activity than the clinical drug ($IC_{50} = 2.3 \pm 0.2 \mu M$ for 2 versus $3.6 \pm 0.5 \mu M$ for cisplatin). Moreover, an enhancement of the antitumor response is achieved when adding an equimolar amount of alkali metal chloride (NaCl or KCl) to the medium, for instance, testing compound 1 against the cisplatin-resistant A2780cis cells, the IC_{50} decreases from 9.3 ± 0.4 to 7.4 ± 0.3 and $5.4 \pm 0.1 \mu M$, respectively, after addition of the salt solution. For the platinum derivative 2, the IC_{50} improves by ca. 40% reaching $1.3 \pm 0.1 \mu M$ when potassium chloride is added. Likewise, the resistant factor found for 2 ($RF = 1$) confirms that this complex circumvents cisplatin-resistance in A2780cis and is improved with the addition of potassium chloride ($RF = 0.65$). The presence of the aza crown ether moiety as linker in the systems studied herein is a key point since, in addition to allowing and facilitating interaction with alkali metal ions, this unit is flexible enough to adapt to a variety of environments, as confirmed by the X-ray crystal structures described, where different conformations and ways to fold in are found. In order to gain insight into the electronic and structural facts involved in the interaction of complex 2 with the alkali metal ions, a DFT study was performed, and the description of the molecular electrostatic potentials (MEPs) is also presented.



INTRODUCTION

Although many successful advances in the field of cancer treatment have been achieved during the last years, this disease continues to widely affect humanity and remains to be the second leading cause of death after cardiovascular diseases. The cancer death rate is still about one in six deaths.¹ Therefore, it is necessary to continue research focused on the design of antitumor drugs and search for new approaches.

Among the metal-based drugs approved for chemotherapy, platinum complexes are between the most used with almost 50% of all cancer patients treated with them. Cisplatin, *cis*-diaminedichloroplatinum(II), was the first platinum-based antineoplastic drug approved by the FDA, that in 1978 authorized its use for the treatment of testicular and ovarian malignancies.² Nowadays, it is also used to treat cervical, breast, bladder, head, neck, esophageal, and lung cancer, as well as mesothelioma and neuroblastoma, remaining as the most employed metal-based drug in oncology.^{3,4} It is generally

accepted that the chemotherapeutic mechanism of action involves binding of cisplatin to the N7 position of the imidazole ring of the purine bases in DNA—guanine (G) and, to a lesser extent, adenine (A)—to form either monofunctional (via one leaving group) or bifunctional adducts (via both leaving groups), thereby interfering with the DNA replication and causing the cell to undergo apoptosis.^{5–7}

The use and efficacy of platinum-based drugs, however, is limited due to intrinsic and acquired cell resistance after continuous treatment^{8,9} as well as a large number of side

Received: July 13, 2020

effects^{10–12} including nausea, vomiting, ototoxicity, neurotoxicity hemolytic anemia, electrolyte disturbance, and nephrotoxicity. Particularly problematic is the nephrotoxicity,¹³ which originates from the circumstance that cisplatin is mainly excreted through the kidneys. Renal failure may be induced by platinum binding to thiol-containing enzymes provoking their inactivation.¹⁴ Diamine(1,1-cyclobutanedicarboxylato(2-)-O,O')platinum(II) known as carboplatin and *cis*-[(1R,2R)-1,2-cyclohexanediamine-*N,N'*][oxalato(2-)-O,O']platinum(II) named oxaliplatin are second generation platinum-based antineoplastic drugs and are approved for clinical use worldwide. In addition, diamine[hydroxyacetato(2-)-O,O']platinum(II) (nedaplatin), [2-hydroxypropanoato(2-)-O1,O2][1,2-cyclobutanedimethanamine-*N,N'*]platinum(II) (lobaplatin), and [propanedioato(2-)-O,O'] [2-(1-methylethyl)-1,3-dioxolane-4,5-dimethanamine-*N,N'*]platinum(II) (heptaplatin) are also admitted for use in Asia. Although these drugs were introduced to overcome the drawbacks of cisplatin, this has not been entirely achieved.¹⁵

It is nowadays clear that the toxicity and tumor resistance of platinum-based drugs is due to the high affinity of platinum for sulfur donors. It is assumed that this metal ion interacts with sulfur-containing biomolecules such as amino acids (cysteines and methionines), peptides (glutathione), proteins (metallothionein), and others, disrupting their functions.¹⁶ Once inside the cells, cisplatin is activated by binding to water molecules to form a chemically reactive aqua species, which preferentially reacts with systems bearing moieties that include sulfur groups, e.g., cysteine or methionine amino acid residues (tripeptide glutathione or metallothionein). In some platinum-resistant cancer cells, the glutathione and metallothionein levels are elevated, so that activated platinum is effectively “mopped up” in the cytoplasm before DNA binding can occur, thereby causing resistance.⁴

In order to generate metal-based drugs exhibiting high anticancer activity and concomitant reduced toxicity with respect to cisplatin and its analogues, in the last two decades, many research groups have focused toward the study of platinum(II) and palladium(II) complexes containing N- and S-donor ligands. Within this context, dithiocarbamates (dtcs) are versatile ligands that are easily prepared and form a variety of stable complexes with various transition metals, making them excellent candidates for their use in medicine,¹⁷ including anticancer drugs.¹⁸ Marzano and co-workers have reported a class of mixed-ligand platinum(II) complexes based on dithiocarbamates and various amines, exhibiting higher cytotoxicity than cisplatin as well as low nephrotoxicity and null cross-resistance with cisplatin.¹⁹ As a result of the chelate effect, dtc ligands form quite stable complexes with transition metals, which prevents decomposition in physiological media. The strong *trans*-influence of the sulfur atoms potentially avoids the interaction of the metal center with thiol-containing molecules, reducing side effects such as renal toxicity and, in some way, also cell resistance.

On another front, there is increasing evidence that normal and tumor cells exhibit substantial differences with respect to membrane potentials, potassium currents, and ion concentrations that could be exploited for therapy using membrane-active ionophores.²⁰ In particular, the concentration of potassium ions in cancer cells is twice that of normal cells. Crown ethers might be a good option because of the similar behavior to natural ionophores such as gramicidin, valinomycin, and nonactin, some of which were found to be toxic in

prokaryotic and eukaryotic cell systems.²¹ The similarity to natural ionophores results from the fact that they possess a hydrophilic cavity with a hydrophobic periphery, being able to form stable metal ion complexes, which can be incorporated in the lipid fraction of cellular membranes. In addition to reports on functionalized crown ethers capable of binding and cleaving DNA, research within this field has been also focused on compounds that inhibit tumor-cell growth by disrupting potassium ion homeostasis, which, in turn, leads to cell cycle perturbations and apoptosis.²² The cytotoxicity of platinum complexes containing crown ether and aza crown ether platforms has been also examined, although such studies are quite scarce.^{23–28}

Considering these precedents, we feel that crown ether-based dithiocarbamate metal complexes might be a reasonable starting point for designing new antineoplastic platinum drugs. Although a relatively large variety of metal complexes with aza crown ether-dtc ligands have been reported with different purposes,^{29–36} it is surprising that, to date, no platinum or palladium derivative has been described. Herein we present the first examples of aza crown ether-dtc complexes with these metal ions and an evaluation of cytotoxic activity against some human tumor cells, namely HeLa-229 cervix and A2780 ovarian carcinoma cells, as well as against the cisplatin-resistant mutant A2780*cis*. These preliminary results are very promising and provide an interesting novel approach for the design of antitumor metal-based drugs with multiple response.

EXPERIMENTAL SECTION

Materials. All reagents and solvents were purchased from Sigma-Aldrich, Chemical Co., and Merck and used without further purification. Potassium *N,N'*-bis(dithiocarbamate)-1,10-diaza-18-crown-6 (**K₂L**) was synthesized as previously described.³⁷

Physical Methods. Melting points were measured on a Büchi B-540 apparatus. IR spectra were recorded on a NICOLET 6700 FT-IR Thermo Scientific instrument using an ATR accessory in the range of 4000–500 cm⁻¹. Mass spectra of complexes **1** and **2** in methanol were recorded on a Q-TOF AB Sciex QStar Elite equipment using the ESI⁺ technique within a spectral interval 1–2000 *m/z*. Mass spectra (ESI⁺) of both complexes in a mixture of ethanol/water (3:1 *v/v*) were recorded on a Thermo LTQ-Orbitrap Discovery instrument in a spectral interval 400–2000 *m/z*. The mass spectrum of complex **5** was recorded on a JEOL-MStation 700 using the FAB⁺ technique. NMR studies of complexes **1–5** in CDCl₃ were carried out with a Varian Inova 400, Mercury 200, or Bruker AVANCE III HD 500 spectrometer. NMR spectra (¹H and ¹³C) of complexes **1** and **2** in CD₃CD₂OD/D₂O (3:1 *v/v*) and DOSY studies were performed on a Bruker AVANCE III HD 400 MHz apparatus. TMS was used as the standard reference for ¹H and ¹³C NMR spectra.

Synthesis. *Preparation of Complex [LPd₂(PPh₃)₄]Cl₂ (1).* A solution of **K₂L** (0.069 g, 0.14 mmol) in methanol (3 mL) was added dropwise to a solution of [Pd(PPh₃)₂Cl₂] (0.20 g, 0.28 mmol) in 27 mL of chloroform. After stirring for 3 h under reflux, the solution was filtered, and the solvent was evaporated under vacuum. The resulting solid was dissolved in methanol. After filtration, the solvent was evaporated to yield compound **1** as a yellow solid. Single crystals suitable for X-ray diffraction analysis were grown from a saturated methanol solution. Yield: 0.163 g (67%). MP 77–80 °C. IR-ATR (cm⁻¹) 1522 (ν_{C-N}), 1433 (ν_{C-P}), 1093 (ν_{C-S}). ¹H NMR (CDCl₃, 200 MHz) δ = 3.56 (s (br), 8 H1), 3.64 (s (br), 8 H2), 3.97 (s (br), 8 H3), 7.29–7.40 (m, 60 [H6, H7, H8]) ppm. ¹³C{¹H} NMR (CDCl₃, 50 MHz) δ = 69.9 (C1), 67.5 (C2), 50.1 (C3), 203.9 (C4), 133.6 (C6) 131.3 (C5) 128.5 (C7), 127.9 (C8) ppm. ³¹P{¹H} NMR (CDCl₃, 81 MHz) δ = 26.0 ppm. ESI⁺-HRMS (*m/z*) 836.1081; calcd. for [C₈₆H₈₄N₂O₄P₄S₄Pd₂]²⁺: 836.1161.

Table 1. Selected Crystallographic Data for Complexes 1, 3, 4·2CHCl₃, and 5·2CHCl₃

data	1	3	4·2CHCl ₃	5·2CHCl ₃
empirical formula	C ₈₆ H ₈₄ N ₂ Cl _{1.33} Pd ₂ O ₄ P ₄ S ₄	C ₁₃₄ H ₁₂₄ B ₂ N ₂ O ₄ P ₄ Pd ₂ S ₄	C ₁₃₆ H ₁₂₆ B ₂ Cl ₆ N ₂ O ₄ P ₄ Pt ₂ S ₄	C ₅₂ H ₅₆ Cl ₈ N ₂ Ni ₂ O ₄ P ₂ S ₄
formula weight	1722.24	2312.88	2729.0	1364.18
temp/K	100	100	100	296
crystal system	monoclinic	triclinic	monoclinic	orthorhombic
space group	C2/c	P-1	P2 ₁ /n	Pbca
a/Å	50.6792(8)	11.6380(2)	9.5827(2)	11.1233(6)
b/Å	10.7168(1)	12.7897(3)	34.6376(7)	16.4948(9)
c/Å	17.4661(2)	19.7635(4)	18.0933(4)	33.104(2)
α/deg	90	82.378(2)	90	90
β/deg	111.771(2)	77.148(2)	94.345(2)	90
γ/deg	90	76.704(2)	90	90
volume/Å ³	8809.6(2)	2780.8(1)	5988.3(2)	6073.8(6)
Z	4	1	2	4
ρ _{calc} /cm ³	1.299	1.381	1.513	1.492
μ/mm ⁻¹	5.540	4.300	7.134	1.206
F(000)	3808	1200	2760	2800
crystal size/mm ³	0.24 × 0.16 × 0.12	0.18 × 0.16 × 0.12	0.28 × 0.14 × 0.12	0.43 × 0.30 × 0.21
radiation	CuKα (λ = 1.54184)	CuKα (λ = 1.54184)	CuKα (λ = 1.54184)	MoKα (λ = 0.71073)
2θ range for data collection/deg	4.200 to 72.454	3.552 to 72.684	3.538 to 72.756	2.210 to 22.490
index ranges	−61 ≤ h ≤ 61, −13 ≤ k ≤ 10, −21 ≤ l ≤ 19	−13 ≤ h ≤ 7, −15 ≤ k ≤ 14, −23 ≤ l ≤ 21	−11 ≤ h ≤ 11, −40 ≤ k ≤ 42, −22 ≤ l ≤ 21	−14 ≤ h ≤ 14, −19 ≤ k ≤ 22, −44 ≤ l ≤ 44
reflections collected	17788	18909	23775	88358
independent reflections	8517 [R _{int} = 0.0243, R _{sigma} = 0.0333]	10017 [R _{int} = 0.0288, R _{sigma} = 0.0414]	11656 [R _{int} = 0.0467, R _{sigma} = 0.0604]	7566 [R _{int} = 0.0967, R _{sigma} = 0.0577]
data/restraints/parameters	8517/147/525	10017/0/685	11656/0/721	7566/30/371
goodness-of-fit on F ²	1.051	1.017	1.087	1.019
final R indexes [I ≥ 2σ(I)]	R ₁ = 0.0363, wR ₂ = 0.0933	R ₁ = 0.0301, wR ₂ = 0.0745	R ₁ = 0.0678, wR ₂ = 0.1702	R ₁ = 0.0529, wR ₂ = 0.1210
final R indexes [all data]	R ₁ = 0.0392, wR ₂ = 0.0953	R ₁ = 0.0325, wR ₂ = 0.0766	R ₁ = 0.0755, wR ₂ = 0.1755	R ₁ = 0.1302, wR ₂ = 0.1523
largest diff peak/hole/e Å ⁻³	1.184/−0.473	0.767/−0.664	1.932/1.926	0.467/−0.405

Preparation of Complex [LPt₂(PPh₃)₄]Cl₂ (2). To a solution of [Pt(PPh₃)₂Cl₂] (prepared *in situ* from [Pt(PhCN)₂Cl₂] (0.025 g, 0.056 mmol) and PPh₃ (0.028 g, 0.11 mmol) in 27 mL of chloroform under reflux for 1 h) was added dropwise a methanolic solution (3 mL) of K₂L (0.013 g, 0.027 mmol). The resulting reaction mixture was refluxed for an additional 2 h and then filtered, and the solvent was evaporated under vacuum. The resulting solid was dissolved in methanol. After filtration, the solvent was evaporated to yield compound 2 as a colorless solid. Yield: 0.030 g (59%). MP 114–117 °C. IR-ATR (cm⁻¹) 1526 (ν_{C-N}), 1434 (ν_{C-P}), 1095 (ν_{C-S}). ¹H NMR (CDCl₃, 400 MHz) δ = 3.59 (s (br), 8 H1), 3.68 (s (br), 8 H2), 3.91 (s (br), 8 H3), 7.29–7.44 (m, 60 [H6, H7, H8]) ppm. ¹³C{¹H} NMR (CDCl₃, 100 MHz) δ = 70.4 (C1), 67.9 (C2), 51.2 (C3), 202.6 (C4), 132.0 (C5), 134.2 (C6), 128.85 (C7), 128.74 (C8) ppm. ³¹P{¹H} NMR (CDCl₃, 202.42 MHz) δ = 15.11 ppm ¹J_(P-Pt) = 3269 Hz. ESI⁺-HRMS (m/z) 925.1745; calcd. for [C₈₆H₈₄N₂O₄P₄S₄Pt₂]²⁺: 925.1774.

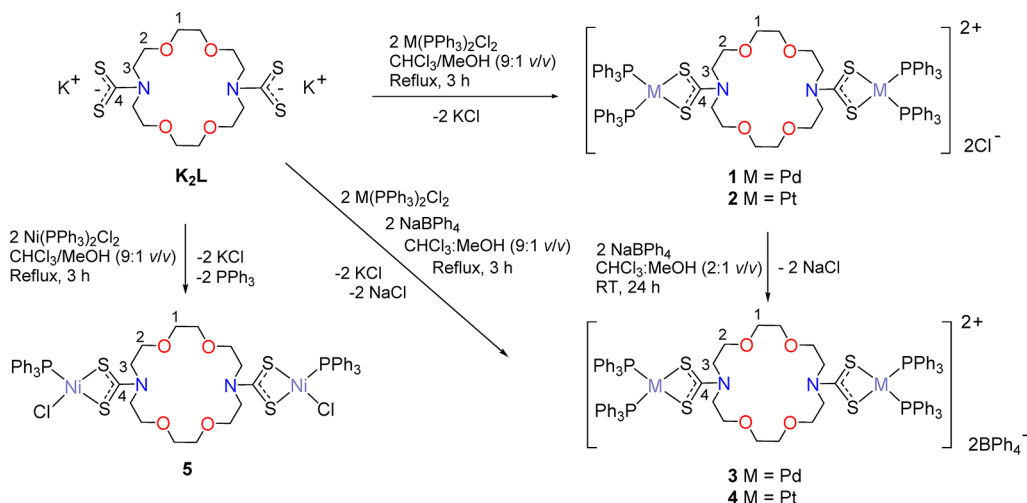
Preparation of Complex [LPd₂(PPh₃)₄](BPh₄)₂ (3). Complex 3 was synthesized by two different procedures: A) A solution of sodium tetraphenylborate (0.0039 g, 0.0114 mmol) in 1 mL of methanol was slowly added to a solution of compound 1 (0.010 g, 0.0057 mmol) in 2 mL of chloroform. The resulting reaction mixture was stirred for 24 h at room temperature and then allowed to slowly evaporate for 2 days, to afford compound 3 as orange crystals. B) A *single-pot* reaction for 3 h under reflux mixing a solution of K₂L (0.007 g, 0.0147 mmol) in methanol (3 mL), [Pd(PPh₃)₂Cl₂] (0.008 g, 0.030 mmol), and NaBPh₄ (0.0100 g, 0.030 mmol) in 27 mL of chloroform: Slow evaporation of the solvent afforded a solid that was extracted with methanol. After filtration and evaporation of methanol under vacuum, the resulting solid was washed with diethyl ether. Crystals suitable for single-crystal X-ray diffraction analysis were grown from a solvent mixture of chloroform and methanol (1:1 v/v). Yield: 9 mg (68%). MP 177–180

°C. IR-ATR (cm⁻¹) 1521 (ν_{C-N}), 1434 (ν_{C-P}), 1094 (ν_{C-S}). ¹H NMR (CDCl₃, 200 MHz) δ = 3.25 (s (br), 8 H1), 3.36 (s (br), 8 H2), 3.68 (s (br), 8 H3), 7.40 (m, 16 H10), 7.15 (m, 60 [H6,7,8]), 6.98 (m, 16 H11), 6.85 (m, 8 H12) ppm. ¹³C{¹H} NMR (CDCl₃, 50 MHz) δ = 204.3 (C4), 70.1 (C1), 67.8 (C2), 50.5 (C3), 136.3 (C5), 134.0 (C6), 128.9 (C7, C8), 164.2 (C9, q, ¹J^(11B-¹³C) = 50 Hz), 131.8 (C10), 125.4 (C11), 121.59 (C12) ppm. ³¹P{¹H} NMR (CDCl₃, 81 MHz) δ = 25.9 ppm. ¹¹B NMR (CDCl₃, 160.46 MHz) δ = −6.4 ppm.

Preparation of Complex [LPt₂(PPh₃)₄](BPh₄)₂ (4). Complex 4 was synthesized by two different procedures, as for 3: A) anion exchange from complex 2 and B) a *single-pot* reaction for 3 h under reflux of a mixture consisting of K₂L (0.007 g, 0.0147 mmol) in methanol (3 mL), NaBPh₄ (0.0100 g, 0.029 mmol), and a solution of [Pt(PPh₃)₂Cl₂] prepared *in situ* from [Pt(CH₃CN)₂Cl₂] (0.010 g, 0.029 mmol) and PPh₃ (0.018 g, 0.069 mmol) in 27 mL of chloroform. Single crystals of formula [LPt₂(PPh₃)₄](BPh₄)₂·2CHCl₃ (4·2CHCl₃) suitable for X-ray diffraction analysis were grown from a solvent mixture of chloroform and methanol (1:1 v/v). Yield: 31 mg (87%). MP 252–255 °C. IR-ATR (cm⁻¹) 1527 (ν_{C-N}), 1434 (ν_{C-P}), 1095 (ν_{C-S}). ¹H NMR (CDCl₃, 500 MHz) δ = 3.17 (s (br), 8 H1), 3.29 (t, ¹J = 5 Hz, 8 H2), 3.51 (t, ¹J = 5 Hz, 8 H3), 7.09–7.29 (m, 60 [H6,7,8]), 7.36 (m, 16 H10), 6.95 (m, 16 H11), 6.78 (m, 8 H12) ppm. ¹³C{¹H} NMR (CDCl₃, 125 MHz) δ = 203.07 (C4), 70.36 (C1), 67.95 (C2), 51.14 (C3), 136.5 (C5), 134.3 (C6), 128.9 (C7), 128.9 (C8), 128.3 (C9), 164.5 (C10, q, ¹J^(11B-¹³C) = 50 Hz), 132.1 (C10), 125.72 (C11), 121.84 (C12) ppm. ³¹P{¹H} NMR (CDCl₃, 81 MHz) δ = 15.14 ppm ¹J_(P-Pt) = 3273 Hz. ¹¹B NMR (CDCl₃, 160.46 MHz) δ = −6.6 ppm.

Preparation of Complex [LNi₂(PPh₃)₂(Cl)₂] (5). A solution of K₂L (0.10 g, 0.20 mmol) and [NiCl₂(PPh₃)₂] (0.26 g, 0.40 mmol) in 50 mL of a mixture of chloroform/methanol (9:1 v:v) was stirred under reflux for 3 h. The resulting green solid was removed by filtration. The residual

Scheme 1. Reaction Sequences for the Preparation of Complexes 1–5



purple solution was then evaporated, giving a solid that was washed twice with hexane to isolate compound **5**. Single crystals of formula $[\text{LNi}_2(\text{PPh}_3)_2(\text{Cl})_2] \cdot 2\text{CHCl}_3$ (**5**·**2CHCl**₃) suitable for X-ray diffraction analysis were grown from a saturated chloroform solution. Yield: 0.173 g (77%). MP 59–62 °C. IR-ATR (cm^{-1}) 1514 ($\nu_{\text{C-N}}$), 1433 ($\nu_{\text{C-P}}$), 1096 ($\nu_{\text{C-S}}$). ¹H NMR (CDCl_3 , 200 MHz) δ = 3.49 (s (br), 8 H1), 3.58 (s (br), 8 H2), 3.78 (s (br), 8 H3), 7.37 (m, 30 [H6–8]) ppm. ¹³C{¹H} NMR (CDCl_3 , 50 MHz) δ = 205.7 (C4), 70.39 (C3), 68.3 (C2), 50.3 (C1), 133.9 (C5), 134.2 (C6), 129.4 (C7), 128.5 (C8) ppm. ³¹P{¹H} NMR (CDCl_3 , 202.46 MHz) δ = 42.7 ppm. ESI⁺-HRMS (m/z) 1087.2037; calcd. for $[\text{C}_{50}\text{H}_{54}\text{ClN}_2\text{Ni}_2\text{O}_4\text{P}_2\text{S}_4]^+$: 1087.0837.

X-ray Crystallography. Intensity data for **1**, **3**, and **4**·**2CHCl**₃ were collected at $T = 100$ K with $\text{Cu-K}\alpha$ radiation ($\lambda = 1.54184$ Å, monochromator: graphite) on an Agilent Technologies SuperNova diffractometer equipped with the EOS2 CCD area detector and an Oxford Instruments Cryogen cooler. The measured intensities were reduced to F^2 and corrected for absorption using spherical harmonics (CrysAlisPro).³⁸ Data for **5**·**2CHCl**₃ were collected using an Enraf Nonius Kappa-CCD instrument at $T = 296$ K with $\text{MoK}\alpha$ radiation ($\lambda = 0.7173$ Å). In all cases, reflection data were corrected for Lorentz and polarization effects. For all compounds, structure solution, refinement, and data output were performed with the OLEX2.2.0³⁹ program package using SHELXL-2014/2015⁴⁰ for the refinement. All non-hydrogen atoms were refined anisotropically. Hydrogen atoms were placed in geometrically calculated positions and constrained with the use of a riding model. Selected crystallographic data are shown in Table 1.

The asymmetric unit of compound $[\text{LPd}_2(\text{PPh}_3)_4]\text{Cl}_2$ (**1**) comprises half of the dicationic dinuclear complex that is located on a crystallographic 2-rotation axis, a chloride anion with an occupancy factor of 0.67 and several electron density peaks that indicate the presence of solvent molecules and an additional chloride. Since the positions of the solvent/chloride could not be assigned with certainty due to rather large solvent cavities (total solvent accessible volume per unit cell = 1390.6 \AA^3 [15.8%]), in the final refinement cycles, the solvent mask methodology⁴¹ implemented in OLEX2 was used for handling the corresponding electron density. In addition, the aza crown ether skeleton is disordered over two positions. Split positions were assigned to the associated atoms, and the occupancy of each conformation was refined, with the sum of the occupancies constrained to unity. The major position, labeled with A, has an occupancy factor of 0.626(15). The disorder was refined using similarity distance and U_{ij} restraints. The asymmetric units of $[\text{LPd}_2(\text{PPh}_3)_4](\text{BPh}_4)_2$ (**3**) and $[\text{LPt}_2(\text{PPh}_3)_4](\text{BPh}_4)_2 \cdot 2\text{CHCl}_3$ (**4**·**2CHCl**₃) comprise half of the dicationic dinuclear complex that is located on a crystallographic inversion center, a tetraphenyl borate anion and, in the case of compound **4**·**2CHCl**₃, additionally a noncoordinated CHCl_3 solvent molecule. Compound **4**·**2CHCl**₃ shows positional disorder that was partially resolved. For the

Pt1 ion, the P atoms of the triphenylphosphine moieties and the S atoms of the dithiocarbamate moiety, two positions were found and refined. The phenyl rings are disordered as well, but the low quality of the crystals prevented definition of the individual positions. The refinement of the highest occupied positions gave an occupation factor of 0.82(1) after including identical U_{ij} constraints for each couple of disordered atoms, except for platinum. In the discussion of the geometry data, only the atoms corresponding to the major molecule fragment are considered. The asymmetric unit of compound $[\text{LNi}_2(\text{PPh}_3)_2\text{Cl}_2] \cdot 2\text{CHCl}_3$ (**5**·**2CHCl**₃) comprises half of the neutral dinuclear complex that is located on a crystallographic inversion center and a noncoordinated CHCl_3 solvent molecule disordered over two positions. The disorder was refined using similarity U_{ij} restraints. Intermolecular distances in the crystal structures of compounds **1** and **3**–**5** were analyzed with MERCURY.⁴²

DFT Calculations. Gaussian 16 revision C.01⁴³ was used for all calculations, using GaussView 6 as a graphical interface. The DFT calculations were performed using the Austin-Frisch-Petersson functional with dispersion (APFD).⁴⁴ For the platinum atom, the Stuttgart–Dresden basis set (SDD), which describes the effective core potential (ECP),⁴⁵ and for the nonmetal atoms, the 6-31G(d) basis set were used to optimize the ground state geometry of the species: $[\text{LPd}_2(\text{PPh}_3)_4]^{2+}$ (conformer **1a**), $[\text{LPt}_2(\text{PPh}_3)_4]^{2+}$ (conformers **2a**, **2b**, **2c**, and **2d**), $[\text{Na}(\text{L})\text{Pt}_2(\text{PPh}_3)_4]^{3+}$ (conformers **2cNa** and **2dNa**), and $[\text{K}(\text{L})\text{Pt}_2(\text{PPh}_3)_4]^{3+}$ (conformer **2dK**).

Throughout this work, solvent effects (ethanol) were included by using the polarizable continuum model (PCM),⁴⁶ in which the solute cavity is built as an envelope of spheres centered on atoms or atomic groups with appropriate radii. In particular, the integral equation formalism (IEFPCM) variant as implemented in Gaussian 16 was used. The stationary points found on the potential energy surfaces resulting from the geometry optimizations were tested to represent energy minima rather than saddle points via frequency analysis. The initial input geometries were adapted from the crystal structures of the compounds.

Molecular Electrostatic Potential (MEP) surfaces were generated with GaussView 6, first generating the Gaussian cube of total electron density obtained from the DFT calculations and then calculating the corresponding ESP mapped surface at the 4×10^{-4} isodensity value.

Cell Lines and Growth Conditions. The human cervix carcinoma cell line HeLa-229 used in this study was kindly provided by Dr. G. Mengod (CSIC-IDIBAPS of Barcelona, Spain). The cisplatin-sensitive human ovarian cancer cell line A2780 and the cisplatin-resistant mutant A2780cis were obtained from the European Collection of Cell Cultures through Sigma-Aldrich Inc. The cells were grown in Dulbecco's Modified Eagle's Medium (DMEM, HeLa-229) or RPMI 1640 medium (A2780 and A2780cis) supplemented with 10% fetal calf serum (FCS) and 2 mM L-glutamine. Cells were maintained in a

continuous logarithmic culture at 37 °C in a humidified atmosphere of 5% CO₂ and were harvested using trypsin-ethylenediaminetetraacetic acid. All media and supplements were purchased from Sigma-RBI, Spain.

In Vitro Chemosensitivity Assays. Cells were seeded into 96-well plates (Beckton-Dickinson, Spain) with a volume of 100 μL (4000 cells/well) and were incubated prior to dosage for 4–6 h (HeLa-229) or 24 h (A2780 and A2780*cis*). Solutions of the Pd (1) and Pt (2) complexes, as well as the corresponding mixtures containing an equivalent portion of NaCl or KCl, in a solvent mixture of ethanol/water (3:1 v/v) were added to the cells. After the appropriate incubation time, i.e., 48 h for HeLa-229 and 96 h for A2780 and A2780*cis*, the cells were fixed by adding 10 μL of MTT [3-(4,5-dimethylthiazol-2-yl)-2,5-diphenyltetrazolium bromide] per well for 4 h. The fixative was then removed, and the wells were washed four times with distilled water. The optical density was measured at 595 nm with a Tecan Ultra Evolution microplate reader.

Each compound was tested using six or seven consecutive dilutions ranging from 50 μM to 0.025 μM. The compound concentration able to inhibit cell growth by 50% with respect to the control, IC₅₀, was then determined from semilogarithmic dose–response sigmoid curves using the GraphPad Prism Ver. 2.01 software (GraphPad Software Inc.). The cytotoxicity of K₂L, Na₂L, and cisplatin (dissolved in ethanol/water, 3:1 v/v) was evaluated for comparison under the same experimental conditions. All compounds were tested in two independent experiments with triplicate points. The *in vitro* studies were performed in the Unit for the Evaluation of Pharmacological Activities of Chemical Compounds of the University of Santiago de Compostela (USC) in Spain.

RESULTS

Synthesis and Characterization of the Complexes.

Potassium *N,N'*-bis(dithiocarbamate)-1,10-diaza-18-crown-6 (K₂L) was prepared from the reaction of 1,10-diaza-18-crown-6, CS₂, and KOH in methanol, employing slight modifications of the methods described in the literature.^{37,47} K₂L was not isolated but used *in situ* for the preparation of the group 10 metal complexes.²⁹ Compounds 1 and 2 were obtained from the reaction of K₂L with 2 equiv of [M(PPh₃)₂Cl₂] (M = Pd, Pt) in the conditions described in the Experimental Section (see Scheme 1). In both cases, solids were isolated in moderate yields. The spectroscopic analysis revealed that the dianionic ligand (L²⁻) is bound to two metal ions. At each metal site two chloride atoms in the starting metal complex were replaced by a dtc moiety from the ligand giving a dinuclear dicationic metal complex, in which the metal centers are coordinated by two sulfur atoms from the dtc ligand in a κ²-S chelating fashion and two monodentate triphenylphosphine molecules. Two chloride counterions neutralize the complexes, yielding [LPd₂(PPh₃)₄]Cl₂ (1) and [LPt₂(PPh₃)₄]Cl₂ (2). Furthermore, chloride anion replacement can be achieved by treatment of compounds 1 and 2 with 2 equiv of NaBPh₄ under stirring in methanol, affording [LPd₂(PPh₃)₄](BPh₄)₂ (3) and [LPt₂(PPh₃)₄](BPh₄)₂ (4), respectively. Compounds 3 and 4 could also be obtained in a single-pot procedure using [M(PPh₃)₂Cl₂], K₂L, and NaBPh₄ as starting materials in a 2:1:2 stoichiometric ratio and refluxing the corresponding reagent mixture. The nickel derivative 5 was obtained using a procedure similar to the preparation of compounds 1 and 2. However, in this case, a single chloride anion and a triphenylphosphine molecule are replaced by κ²-S,S-chelating dtc groups, leading to the neutral complex [LNi₂(PPh₃)₂Cl₂] (5). The distinct reaction behavior of [Ni(PPh₃)₂Cl₂] compared to the heavier group 10 analogs with Pd(II) and Pt(II) is in agreement with the findings for related Ni(II) derivatives^{48–51} and attributable to the *trans*-effect.

Complexes 1 and 2 are soluble in dmsO, acetonitrile, chloroform, methanol, and a mixture of ethanol/water (3:1 v/v), while complexes 3 and 4 are soluble in methanol and chloroform. Meanwhile, complex 5 is only soluble in chloroform and is not stable in protic solvents, as also found previously for analogous compounds.⁵²

Conclusive evidence for the formation of compounds 1–5 was obtained from the spectroscopic and mass spectrometric analysis. The ESI⁺-mass spectra of complexes 1 and 2 showed peaks for mass clusters at *m/z* 836.11 and 925.66, corresponding to the dicationic species [LM₂(PPh₃)₄]²⁺, respectively. The complex compositions were further established by high-resolution mass spectrometry (HRMS), giving *m/z* values of 836.1081 (calcd.: 836.1161) and 925.1745 (calcd.: 925.1774) for complexes 1 and 2, respectively. As products of the chloride-tetraphenylborate anion exchange, compounds 3 and 4 exhibited mass clusters in the same region as complexes 1 and 2, respectively. In the case of complex 5, a mass cluster was observed at *m/z* = 1087.2037 (calcd. for [LNi₂(PPh₃)₂Cl]⁺: 1087.08370), providing evidence for the loss of a chloride ligand from the neutral molecular compound. Meanwhile, analysis of 1–5 by IR-ATR spectroscopy revealed bands typical for metal-coordinated dtc ligands. The bands for the ν(N–CS₂) stretching vibration were observed between 1514 and 1527 cm⁻¹, while those for the ν(C–S) vibration were detected in the range 1093–1096 cm⁻¹. The bands at approximately 1430 cm⁻¹ are typical for metal-coordinated triphenylphosphine ligands [ν(P–C)]. These results agree with the proposed structures.^{29,37}

The NMR spectroscopic data (CDCl₃) are also consistent with the values reported for analogous systems.^{29,37} For instance, the ¹H NMR spectrum of ligand K₂L shows a single peak at δ = 3.48 ppm for the central OCH₂ group (H1, see Scheme 1) and two triplets at δ = 3.63 and 4.22 ppm for the –OCH₂CH₂N– groups (H2 and H3, Scheme 1). These signals show slight shifts upon complexation with palladium or platinum. For complexes 1 and 2, the singlet signal corresponding to H1 shifts to 3.56 and 3.59 ppm, respectively, whereas the two triplet signals appear at 3.64 (H2)/3.97 (H3) ppm for 1 and 3.68 (H2)/3.91 (H3) ppm for 2. The chemical shifts are different in the presence of [BPh₄]⁻ as counterions, and the corresponding signals were observed at δ = 3.25/3.17, 3.36/3.29, and 3.68/3.51 ppm for compounds 3 and 4, respectively. For the neutral complex 5, the chemical shifts for H1, H2, and H3 were δ = 3.49, 3.58, and 3.78 ppm, respectively. In addition, the DOSY-NMR spectrum of complex 2 evidenced the presence of a single species in solution in both chloroform and the mixture of ethanol/water (3:1 v/v).

The above-described analysis was complemented by the ¹³C{¹H} NMR studies that revealed significant chemical shift changes of the dithiocarbamate carbon atom in the group 10 metal complexes compared with the ligand precursor K₂L (δ = 214.00 ppm). For the five complexes, the signal was shifted to lower frequency by about 10 ppm, i.e., δ = 203.9 (1), 202.6 (2), 204.3 (3), 203.0 (4), and 205.7 ppm (5), confirming the coordination of the CS₂ moiety to the metal center.²⁹ The upfield shift can be attributed to shielding of the NCS₂ carbon by electron donation from the nitrogen after coordination of the sulfur atoms to the metal.

The presence of the PPh₃ ligands in compounds 1–5 was confirmed by ³¹P{¹H} NMR, which revealed signals at δ = 26.0 and 25.9 ppm for the Pd(II) derivatives 1 and 3; meanwhile, for the Pt(II) derivatives, the signals were observed at higher field (δ = 15.11 and 15.14 ppm for species 2 and 4, respectively). For

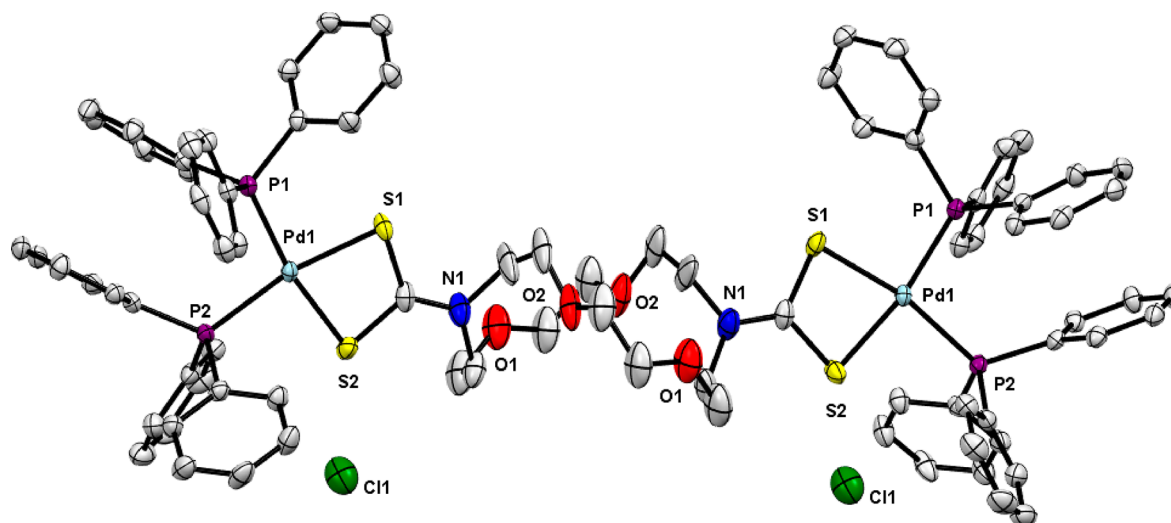


Figure 1. Crystal structure of 1. The disorder part, hydrogen atoms, and solvent molecules are omitted for clarity.

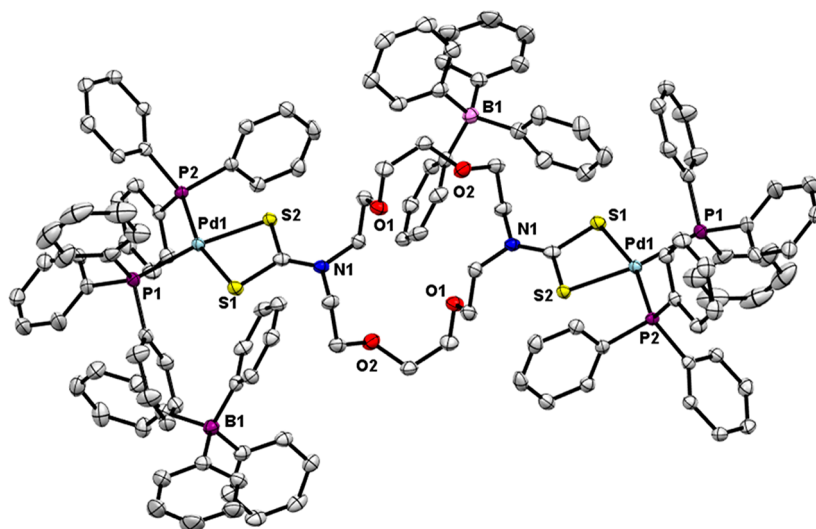


Figure 2. Crystal structure of 3. Hydrogen atoms are omitted for clarity.

compound 5, the ^{31}P NMR signal was shifted to $\delta = 42.7$ ppm, owing to the different chemical environments. Finally, the successful anion exchange in compounds 3 and 4 was confirmed also by ^{11}B NMR experiments, showing signals at $\delta = -6.4$ and -6.6 ppm for 3 and 4, respectively, corresponding to four-coordinate environments of the boron atom.

X-ray Crystallographic Study. Single crystals of compounds 1, 3, 4, and 5 suitable for X-ray diffraction studies were obtained under the conditions described in the [Experimental Section](#). Data were collected at 100 K except for compound 5, which was characterized at room temperature (296 K). The crystal structure analysis revealed that compounds 1, 4, and 5 incorporated noncoordinated solvent molecules in the crystal lattice. Although the solid-state structures of constitutional isomers with Pd(II) and Pt(II) are frequently isostructural,^{53,54} in the case of compounds 3 and 4, two different crystal structures were found, albeit both complexes were crystallized under similar conditions and from the same solvent mixture. Compound 3 crystallized in the triclinic space group $P\bar{1}$ and contains aside from the tetraphenylborate counterions only dicationic dinuclear complex molecules of formula $[\text{LPd}_2(\text{PPh}_3)_4]^{2+}$ with crystallographic inversion symmetry.

On the contrary, compound 4 crystallized in the monoclinic space group $P2_1/n$ in the form of a solvate of composition $[\text{LPt}_2(\text{PPh}_3)_4](\text{BPh}_4)_2 \cdot 2\text{CHCl}_3$ ($4 \cdot 2\text{CHCl}_3$). [Figures 1–4](#) show the molecular structures for compounds 1, 3, 4, and 5, respectively. Crystallographic data and refinement parameters for the crystal structures are given in [Table 1](#). Selected bond distances and angles are given in [Table 2](#).

The molecular structures of compounds 1, 3, and 4 consist of a dicationic metal-coordinated diaza crown bis-dtc skeleton (L) with two chloride (1) or two tetraphenylborate anions (3 and 4) as counterions. In the three compounds, the metal center is embedded in a square-planar geometry with a bidentate dtc moiety coordinated in a $\kappa^2\text{-S-S}'$ -chelating mode and two PPh_3 ligands. In compound 5, the aza crown ether-dtc ligand (L^{2-}) is bound similarly, but the coordination sphere is now completed by one PPh_3 and one chloride ligand.

In the potassium salt K_2L , the S–C–S angle has a value of $121.39(9)^\circ$.³⁷ This angle decreases when coordinated to the group 10 metal atoms [$111.4(2)^\circ$ for 1, $111.2(1)^\circ$ for 3, $111.6(5)^\circ$ for 4, and $108.5(2)^\circ$ for 5]. The smaller S–C–S angle found in 5 enlarges the S–M–S bite angle ($78.256(4)^\circ$) compared to those found in platinum and palladium derivatives

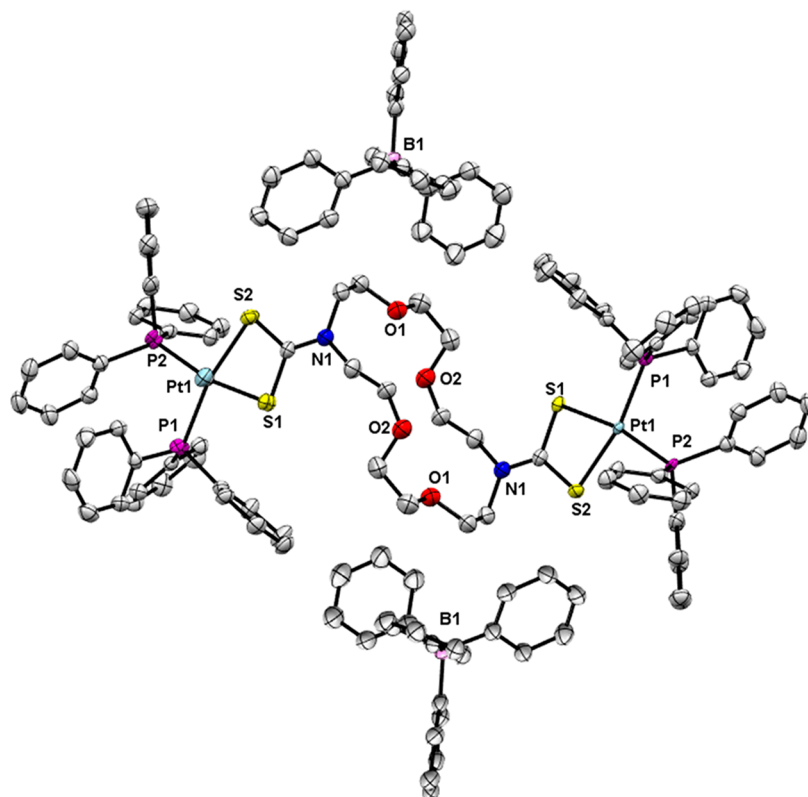


Figure 3. Crystal structure of 4. Hydrogen atoms and solvent molecules are omitted for clarity.

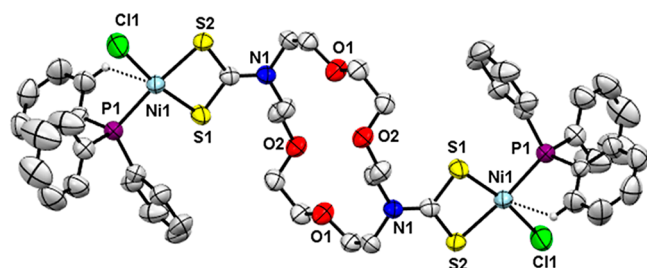


Figure 4. Crystal structure of 5. Hydrogen atoms (except those involved in intramolecular C–H...Ni anagostic interactions) and CHCl₃ solvate molecules are omitted for clarity.

[74.82(3)° (1), 74.83(2)° (3), and 75.1(2)° (4)]. As a consequence of the chelate-type bonding of the dtc groups, a significant distortion from ideal square-planar geometry around the metal centers is generated. The C–S bond distances in compounds 1, 3, 4, and 5 are similar, with values ranging from

1.701(4) to 1.735(9) Å. In contrast, the M–S bond distances are different for each complex, as expected for the different ionic radii of the different metal ions (Table 2). The dtc groups adopt an asymmetric bidentate coordination mode to the metal atoms in 3 and 5, where the M–S bond distances are different, i.e., 2.3627(5)/2.3175(5) and 2.231(1)/2.166(1) Å, approaching a somewhat anisobidentate character. Meanwhile, in the case of compounds 1 and 4, the M–S bond distances are practically identical with values of 2.3338(7)/2.3536(7) Å and 2.341(4)/2.365(5) Å, respectively. The M–P bond distances (2.2960(7)/2.3192(7) Å for 1, 2.3377(5)/2.3365(5) Å for 3, 2.285(3)/2.293(4) Å for 4, and 2.216(1) Å for 5) are in accordance with other related metal complexes.⁵⁵

Concerning the aza crown ether-dtc ligand conformation, the X-ray diffraction analysis shows that in all compounds the two pendants are oriented in an *anti*-disposition (Figure 5); however, the aza crown ether moiety adopts different conformations and crystallographic symmetry. Compounds 4 and 5 exhibit a *quasi-chair* conformation⁵⁶ with crystallographic

Table 2. Selected Bond Distances (Å) and Angles (deg) for Compounds 1, 3, 4, and 5

compd	M–S	M–P	M–Cl	C–S	C–N	S–M–S	S–C–S
K ₂ L (ref 37)	4.1313(5)			1.719(2)	1.354(2)		121.39(9)
	3.3447(5)			1.710(2)			
1	2.3338(7)	2.2960(7)		1.733(3)	1.309(4)	74.82(3)	111.4(2)
	2.3536(7)	2.3192(7)		1.715(3)			
3	2.3627(5)	2.3377(5)		1.724(2)	1.313(3)	74.83(2)	111.2(1)
	2.3175(5)	2.3365(5)		1.723(2)			
4	2.341(4)	2.285(3)		1.734(9)	1.32(1)	75.1(2)	111.6(5)
	2.365(5)	2.293(4)		1.735(9)			
5	2.231(1)	2.216(1)	2.167(1)	1.701(4)	1.315(4)	78.25(4)	108.5(2)
	2.166(1)			1.720(3)			

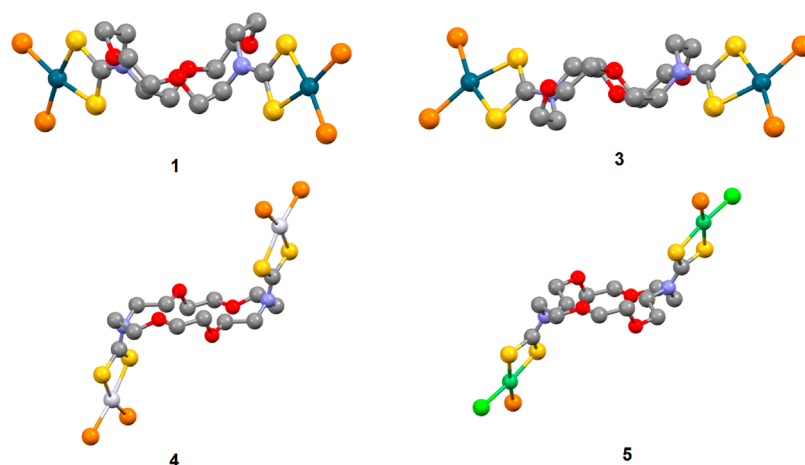


Figure 5. Comparison of the conformations in the aza crown ether skeletons of complexes 1, 3, 4, and 5.

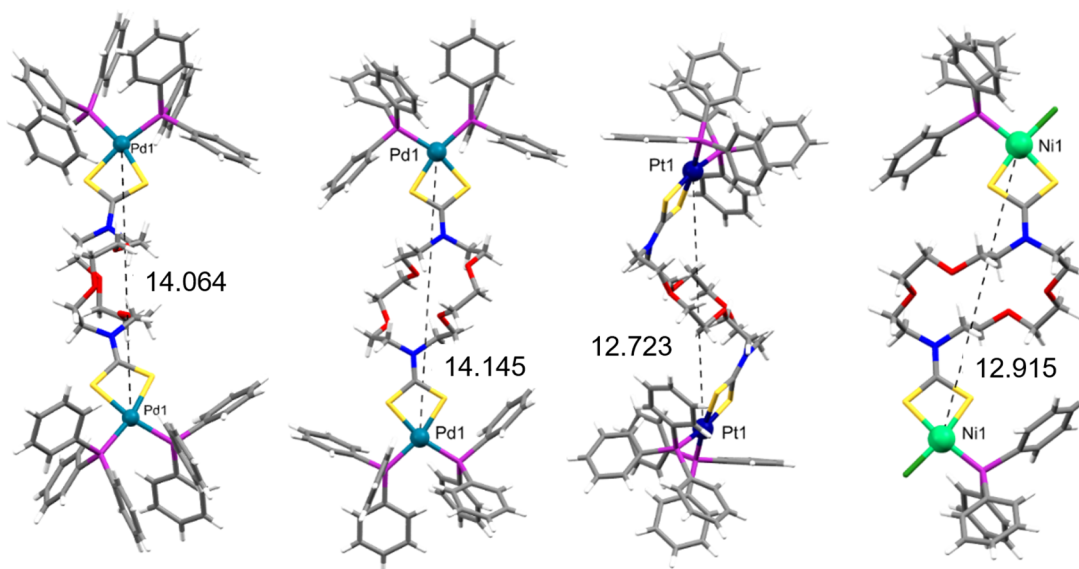


Figure 6. Comparison of the M...M distances (in Å) in complexes 1, 3, 4, and 5.

inversion symmetry; meanwhile, compound 1 has the classic *nest* conformation for crown ethers with crystallographic 2-symmetry, whereas in compound 3 a *chair-chair* conformation with crystallographic inversion symmetry is observed.⁵⁷ The different conformations as well as the different metal sizes in the complexes lead to variations of the metal...metal distances, giving values of 14.064, 14.145, 12.723, and 12.915 Å for complexes 1, 3, 4, and 5, respectively (Figure 6). Noteworthy, compound 5 exhibits a C–H...Ni anagostic interaction, where a hydrogen atom of a phosphine phenyl group interacts with the nickel atom. The H...Ni distance of 2.785 Å is significantly smaller than the sum of the van der Waals radii [3.14 Å].⁵⁸ The C–H...Ni bond angle is 121.90° (Figure 4). Interestingly, a supramolecular aggregate is formed in the crystal structure of the platinum compound 4 by means of C–H...O, C–H...Cl, and Cl...S contacts with the two chloroform molecules enclosed in the cavity (Figure 7). Furthermore, intramolecular C–H...Pt interactions are also found (3.246 Å), which are shorter than the sum of the reported van der Waals radii (3.26 Å).⁵⁸ This chemistry constitutes an active area of research since C–H...M interactions are interesting from the perspective of applications in C–H activation.⁵⁹

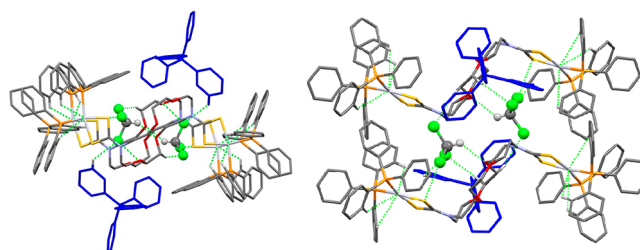


Figure 7. Two perspective views of the supramolecular aggregate (with CHCl₃) in the crystal structure of compound 4 formed by means of C–H...O, C–H...Cl, Cl...S, and eventually C–H...Pt interactions. The BPh₄[−] anions are shown in blue.

Cytotoxicity and Resistant Profiles. The isostructural molecular complexes 1 and 2 containing palladium and platinum, respectively, were tested for cytotoxicity by determination of the IC₅₀ values against the human cervix carcinoma cell line HeLa-229, the human ovarian carcinoma cell line A2780, and cisplatin-resistant mutant A2780*cis* cells. The A2780*cis* cell line exhibits a multifactorial resistance effect to cisplatin including decreased uptake, enhanced DNA repair/tolerance, and elevated GSH levels,^{60,61} making it very useful for testing

Table 3. Cytotoxicity of Compounds 1 and 2 and Their Mixtures with Alkali Metal Chlorides against the Human Cancer Cell Lines HeLa-229, A2780, and A2780cis

compound	IC ₅₀ (μM)			RF ^a
	HeLa-229	A2780	A2780cis	
1	11.0 ± 2	4.1 ± 0.3	9.3 ± 0.4	2.2
2	6.4 ± 0.2	2.2 ± 0.2	2.3 ± 0.2	1.0
[1+NaCl] (1:1)	7.9 ± 0.2	3.7 ± 0.2	7.4 ± 0.3	2.0
[2+NaCl] (1:1)	0.8 ± 0.4	2.1 ± 0.3	2.9 ± 0.2	1.4
[1+KCl] (1:1)	6.8 ± 0.3	4.2 ± 0.3	5.4 ± 0.1	1.3
[2+KCl] (1:1)	2.1 ± 0.2	2.0 ± 0.1	1.3 ± 0.1	0.65
cisplatin	0.53 ± 0.6	0.44 ± 0.06	3.6 ± 0.5	8.2

^aRF = IC₅₀(A2780cis)/IC₅₀(A2780).

alternative drugs. The results are given in Table 3 and depicted in graphic representations in Figures 8 and 9, where the values are compared with those found for the platinum anticancer drug cisplatin under the same experimental conditions. The cytotoxicity assays were performed using ethanol/water (3:1 v/v) as solvent (see the Experimental Section). ESI⁺ mass spectrometry and NMR spectroscopy confirmed the stability of compounds 1 and 2 in this solvent mixture. As indicated above, unfortunately, the nickel compound (5) is not stable in protic solvents, thus having prevented the carrying out of the corresponding cytotoxicity assays. Compounds 1 and 2 exhibit significant cytotoxic activity toward the three cancer cell lines, with low micromolar IC₅₀ values that are comparable to cisplatin. In the three cell lines, the Pt(II) complex 2 shows higher cytotoxicity than the Pd(II) analogue 1. Moreover,

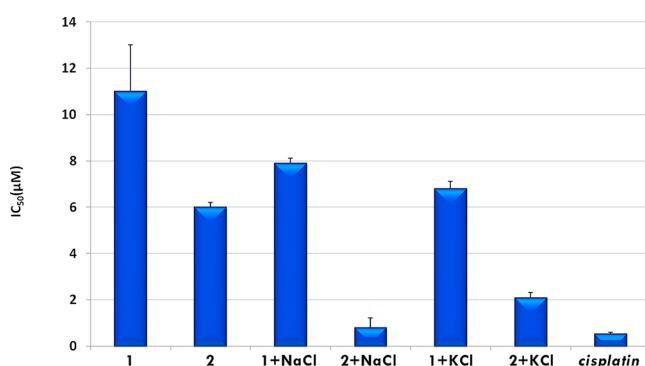


Figure 8. *In vitro* cytotoxic activity of complexes 1 and 2 and their mixtures with alkali metal chlorides against the human cancer cell line HeLa-229.

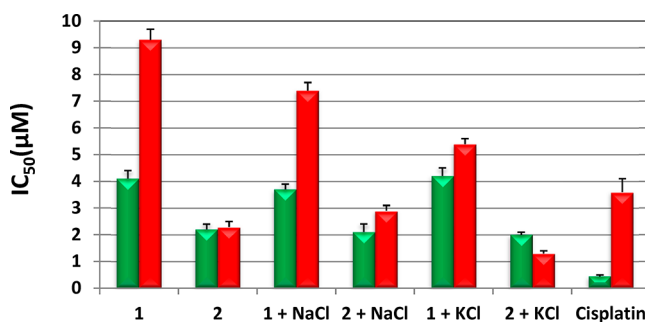


Figure 9. *In vitro* cytotoxic activity of complexes 1 and 2 and their mixtures with alkali metal chlorides against the human cancer cell lines A2780 (green bar) and A2780cis (red bar).

against the cisplatin resistant cell line A2780cis, compound 2 exhibits even better cytotoxic activity than the clinical drug [IC₅₀ = 2.3 ± 0.2 μM for 2 versus 3.6 ± 0.5 μM for cisplatin]. Considering the potential antitumoral activity of certain uncoordinated crown ethers because of their ability to disrupt potassium ion homeostasis,²² the antitumor activity of the alkali metal salts of the aza crown ether-dtc ligand (Na₂L and K₂L) was also evaluated. Inactivity was found for both of them, allowing us to conclude that the presence of the d⁸ metal ions (Pt or Pd) is determinant.

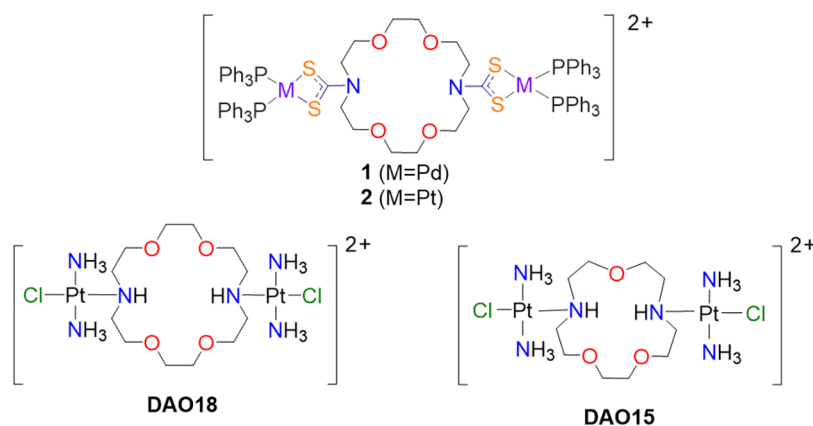
Taking into account the capability of the crown ether moieties to interact with alkali metal ions, we decided to assess if the presence of Na⁺ or K⁺ has an effect on the cytotoxic activity of 1 and 2. Interestingly, the antitumor response of compounds 1 and 2 improved with addition of an equimolar amount of NaCl or KCl to the complex solutions. Against the HeLa-229 cell line, in the case of the palladium compound, the IC₅₀ value decreased from 11.0 ± 2 to 7.9 ± 0.2 and 6.8 ± 0.3 μM with the addition of NaCl and KCl, respectively, whereas in the case of the platinum derivative, the enhancement in the cytotoxic activity was even higher (70–90%), reaching an IC₅₀ of 0.8 ± 0.4 μM with the addition of NaCl, that is similar to the value determined for cisplatin [0.53 ± 0.06 μM]. Against the human ovarian carcinoma cell A2780, the addition of the alkali metal chloride was less effective, but against the cisplatin-resistant A2780cis, an improvement was observed. The IC₅₀ value decreases with the addition of NaCl or KCl to the palladium complex 1 (IC₅₀ = 9.3 ± 0.4, 7.4 ± 0.3, and 5.4 ± 0.1 μM, respectively), and for the platinum complex 2, the cytotoxic activity overcomes the one of cisplatin when potassium chloride is added [IC₅₀ improves ca. 40% reaching 1.3 ± 0.1 μM].

The ability of compounds 1 and 2 (and their mixture with alkali metal chlorides) to circumvent cisplatin-acquired resistance can be described by the resistance factor (RF), which is defined as the ratio of IC₅₀ (resistant cell line) to IC₅₀ (parent cell line). An RF value less than two (RF < 2), is considered to denote non-cross-resistance.⁶² The values given in Table 3 show that the binuclear platinum complex 2 overcomes resistance for A2780cis (RF = 1), while the palladium complex 1 is close to the limit. Addition of alkali metal chloride maintains and/or even enhances the RF values, which decrease to 0.65 and 1.3 upon addition of potassium chloride to solutions of 2 and 1, respectively.

DISCUSSION

In spite of the usefulness of cisplatin and its analogues approved for clinical uses, there are still many challenges to solve in order to overcome their drawbacks, with the development of cellular resistance probably being the most important issue. Tumor resistance to cisplatin is mostly related to decreased membrane transport of the drug, increased cytoplasmic detoxification, and increased DNA repair and tolerance to DNA damage. Therefore, in order to find platinum-based anticancer drugs capable of responding simultaneously to all these fronts, new approaches and fine-tune tailoring design are necessary. It is well-accepted that the increased DNA repair and tolerance to DNA damage is related with the binding mode of the metal-drug to DNA. In order to overcome this inconvenience, polynuclear complexes containing two or more metal centers covalently connected by appropriate linkers have emerged as promising anticancer compounds due to their ability to provide new action modes with the biomolecular targets. The binding of the polynuclear platinum complexes with DNA is clearly different

Scheme 2. Cationic Units Present in 1, 2, DAO18, and DAO15



from that of cisplatin and its analogues, being characterized by flexible, nondirectional DNA adduct formation with a large occurrence of interstrand (versus intrastrand) adducts, as well as the ability to induce DNA conformational changes. On the other hand, cytoplasmic detoxification is originated from the increased levels of thiol-containing species (i.e., glutathione and metallothioneine), which are avidly bonded by platinum. In this way, dithiocarbamates were found as excellent candidates for the preparation of antineoplastic platinum drugs thanks to the strong *trans*-influencing effect of the sulfur atoms which prevents the coordination of the metal to the sulfur atoms of the cytoplasmic proteins. Within this context, the results of the cytotoxicity and resistance profile presented herein support that aza crown ether-dtc ligands are excellent candidates for the design of metal-based drugs able to give multiple response to cell resistance. In particular, the presence of the diaza crown moiety (that plays the role of a linker in the binuclear scaffold) seems to be a determinant key point for the activity since the platform can coordinate to alkali metal ions and act as ionophore. At the same time, there might be a potential effect during the cellular uptake of the agent. It is well-known that the uptake of cisplatin is influenced by factors such as sodium and potassium ion concentration, and the participation of transporter molecules or gated channels has been postulated in addition to passive diffusion. In 2002, Jansen et al.²⁷ described the possibility of incorporating a diaza crown ether as linker in binuclear platinum complexes. They assessed the antitumor response of compounds DAO18 and DAO15 (see Scheme 2) against cell lines A2780 and 2780*cis* but did not find cytotoxicity, so that the idea of using aza crowns as linkers for the design of binuclear antineoplastic metal-drugs was abandoned. However, our results herein presented indicate that an adequate functionalization of the ether moiety as well as an appropriate coordination sphere around the metal ion, including phosphine groups instead of the typical chloride leaving groups (see Scheme 2), can lead to promising systems. Regarding the phosphine groups, it has been reported that their presence in Pt(II) and Pd(II) compounds seems to regulate the lipophilicity of the complexes.⁶³

The data presented in Table 3 show that the addition of alkali metal chloride (NaCl or KCl) to the binuclear palladium and platinum complexes (**1** and **2**) enhances the cytotoxic activity and helps to overcome the resistance in A2780*cis*. In order to gain insight into the origins of this fact as well as to assess the ability of the aza crown moiety to coordinate and stabilize alkali metal ions, a DFT computational study (APFD/SDD/6-31G(d) level) was performed on the binuclear platinum species

$[\text{LPt}_2(\text{PPh}_3)_4]^{2+}$ and the alkali metal complexes $[\text{Na}(\text{L})\text{Pt}_2(\text{PPh}_3)_4]^{3+}$ and $[\text{K}(\text{L})\text{Pt}_2(\text{PPh}_3)_4]^{3+}$. The DFT optimized geometries in ethanol solution for the calculated conformers, namely **2a**, **2b**, **2c**, **2d**, **2cNa**, **2dNa**, and **2dK**, are shown in Figure 10, while selected bond angles and distances (Table S1), together with the optimized Cartesian coordinates (Tables S3–

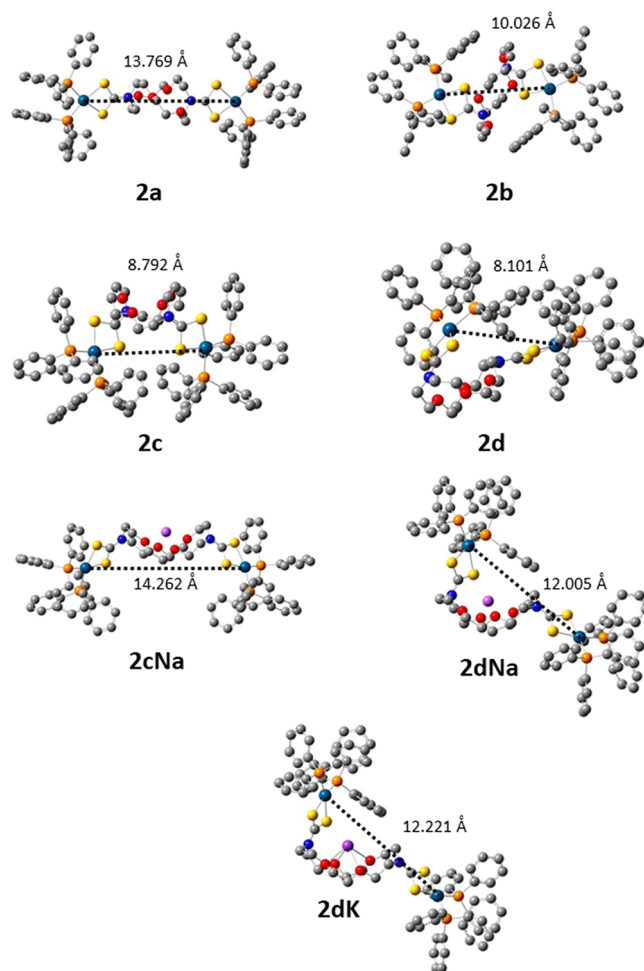


Figure 10. DFT optimized structures of $[\text{LPt}_2(\text{PPh}_3)_4]^{2+}$ (conformers **2a**, **2b**, **2c**, and **2d**), $[\text{Na}(\text{L})\text{Pt}_2(\text{PPh}_3)_4]^{3+}$ (conformers **2cNa** and **2dNa**), and $[\text{K}(\text{L})\text{Pt}_2(\text{PPh}_3)_4]^{3+}$ (conformer **2dK**), indicating the intramolecular Pt...Pt distances. [Hydrogen atoms are omitted for clarity.]

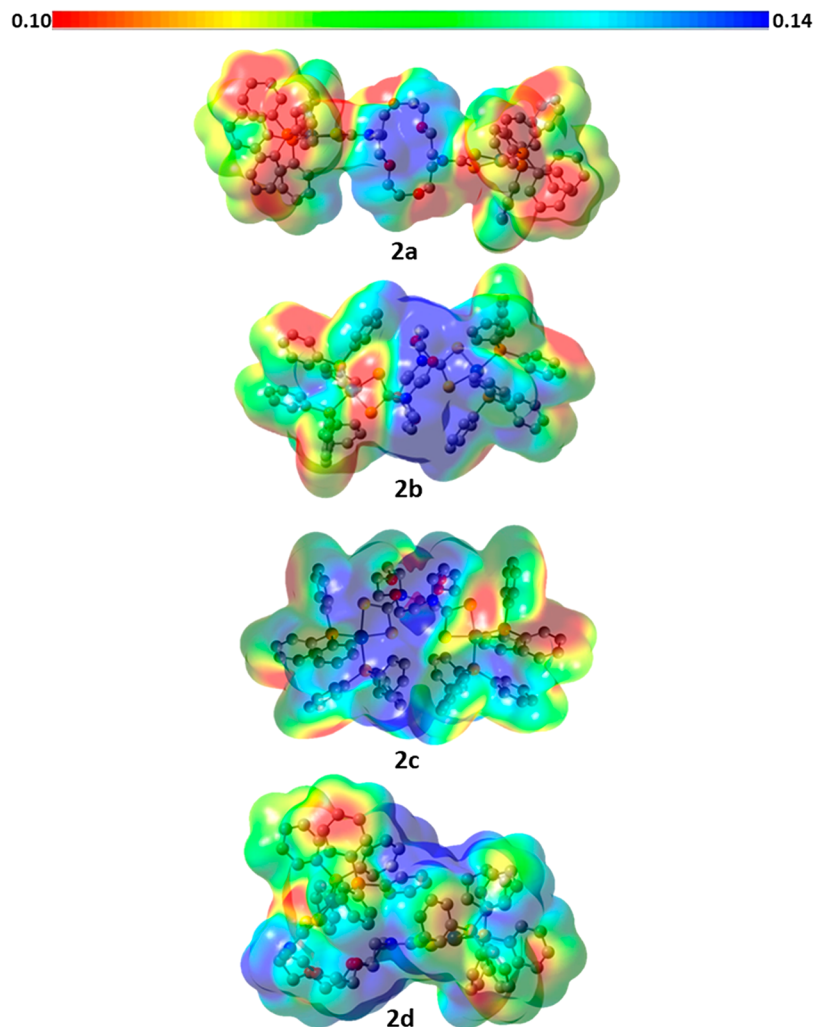


Figure 11. Electrostatic potential maps for $[\text{LPt}_2(\text{PPh}_3)_4]^{2+}$ (conformers **2a**, **2b**, **2c**, and **2d**).

S9), are given in the [Supporting Information](#). Since there are many conformers available for $[\text{LPt}_2(\text{PPh}_3)_4]^{2+}$, calculations were focused to symmetric systems considering the observations in solution by NMR spectroscopy. In addition, and in order to include a comparative study based on different conformations derived from the aza crown ether moiety, we used the X-ray crystal structures of **4** and **1**, that in the latter case was conveniently adapted including platinum instead of palladium, as input geometries for **2b** and **2a**, respectively. Both provided two minimum-energy geometries, with the conformation of **2b** being slightly more stable than that of **2a** [by 2.13 kcal·mol⁻¹ (8.93 kJ·mol⁻¹)]. The *chair* (**2b**) and *nest* (**2a**) conformations are maintained in the optimized geometries, but a comparison between the calculated structure of **2b** and the crystal X-ray structure of **4** illustrated that crystal packing effects have an important effect on the folding of the aza crown ether moiety, allowing for a considerably closer proximity of the platinum atoms in the absence of such packing effects (Pt···Pt, 10.026 Å in **2b** versus 12.723 Å in **4**). The incorporation of alkali metal ions (Na⁺ or K⁺) in the binuclear platinum system necessarily requires a modification of the linker geometry in order to make the aza crown ether accessible for the sodium/potassium ion. Conformers **2cNa** (symmetric) and **2dNa** (asymmetric) represent the minimum energy geometries, being that the asymmetric version is more stable by 1.69 kcal·mol⁻¹ (7.09 kJ·

mol⁻¹). Moreover, in the case of the potassium complex, only the asymmetric conformer **2dK** leads to a minimum of energy, while optimization of the analogous symmetrical conformer **2cK** failed systematically. The molecular geometries of **2dNa** and **2dK** are similar, with Pt···Pt distances of 12.005 and 12.221 Å, respectively, whereas in symmetrical **2cNa**, the linker is more elongated, and the platinum ions are separated by 14.262 Å. The related symmetrical and asymmetrical conformers of **2c** and **2d** for $[\text{LPt}_2(\text{PPh}_3)_4]^{2+}$ were then also optimized, finding **2d** to be more stable than the symmetric analogues **2a**, **2b**, and **2c**. A *nest* conformation of the aza crown ether moiety is present in the three alkali metal complexes (**2cNa**, **2dNa**, and **2dK**), as expected, whereas in the absence of the alkali metal ion, the system evolves to a geometry in which the aza crown ether linker is compressed, which, in turn, moves the platinum ions toward each other (Pt···Pt, 8.792 Å in **2c**, 8.101 Å in **2d**). Overall, the results indicate that the binucleated aza crown ether-dtc ligand L²⁻ is a versatile, flexible platform, which can be easily adapted to different conformations allowing the easy complexation of alkali metal ions. This is an extremely valuable point for the binuclear platinum derivative, which could interact with DNA in different ways.

Figures 11 and **12** show the electrostatic potential maps of the optimized conformers. The molecular electrostatic potential (MEP) at a given point $p(x,y,z)$ in the vicinity of a molecule is

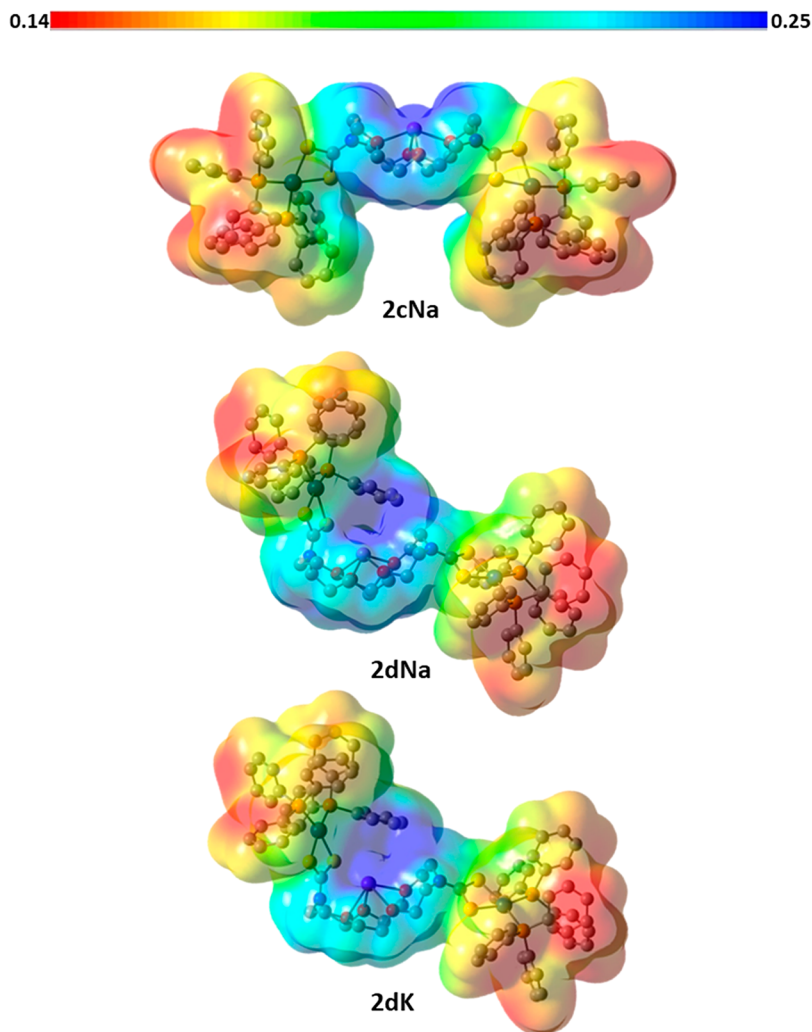


Figure 12. Electrostatic potential maps for $[\text{Na}(\text{L})\text{Pt}_2(\text{PPh}_3)_4]^{3+}$ (conformers **2cNa** and **2dNa**) and $[\text{K}(\text{L})\text{Pt}_2(\text{PPh}_3)_4]^{3+}$ (conformer **2dK**).

the force acting on a positive test charge (a proton) located at p by the electrical charge cloud generated through the molecule electrons and nuclei. It is a good guide in assessing the molecule reactivity toward positively or negatively charged reactants, thus helping in predicting the reactivity of a range of chemical systems for both electrophilic and nucleophilic sites.⁶⁴ A number of chemical interactions, including drug-receptor interactions, can be predicted with the use of MEP.⁶⁴ The values of the electrostatic potential at the surface are represented by different colors, with the potential increasing in the following order: red < orange < yellow < green < light blue < blue. The systems examined herein are cationic, and thus, the potential values are positive in the whole represented range. For the binuclear $[\text{LPt}_2(\text{PPh}_3)_4]^{2+}$ conformers **2a**, **2b**, **2c**, and **2d** (Figure 11), the most positive electrostatic potential (deep blue) is localized inside the aza crown moiety, which is situated in the central part of the molecules in the symmetrical analogues **2a**, **2b**, and **2c** but more to one section of the platform in **2d**. In the latter, an additional important nucleophilic region, apparently related with the platinum metal ions, is also found. Coordination of the alkali metal ion to the crown significantly increases the positive potential values, as shown in Figure 12, therefore, also increasing the affinity of the complexes with anionic species, such as the polyanionic phosphate backbone of DNA as well as anionic proteins present in the cell membrane. In **2cNa**, this region is

accessible for nucleophilic species. In the six conformers, the least positive (red) regions of the MEP maps are localized around the phenyl groups of the PPh_3 ligands, although additional regions at two oxygen atoms of the aza crown moiety, which are clearly pointing outward, are found in **2a**.

CONCLUSIONS

The results here presented show that the ligand N,N' -bis(dithiocarbamate)-1,10-diaza-18-crown-6 (L^{2-}), which contains dithiocarbamate groups directly linked to the nitrogen atoms of an aza crown ether unit, is able to form binuclear complexes with d^8 metal ions (Ni-triade elements), revealing an excellent option and starting point for the design of metal-based drugs able to circumvent cisplatin-resistance. Decreased cellular uptake, enhanced DNA repair/tolerance, and elevated GSH levels are the main factors involved in cell resistance and must be taken into consideration simultaneously when dealing with this issue. The binuclear platinum complex **2** exhibits better cytotoxic activity against the cisplatin resistant cell line A2780cis than the clinical drug ($\text{IC}_{50} = 2.3 \pm 0.2 \mu\text{M}$ for **2** versus $3.6 \pm 0.5 \mu\text{M}$ for cisplatin), and the resistant factor ($\text{RF} = 1$) confirms that this complex circumvents cisplatin-resistance in this cell line. An additional enhancement of the antitumor response is achieved when adding an equimolar amount of alkali metal chloride (NaCl or KCl) to the complex, evidencing that

the presence of the aza crown moiety in the system is a key point. This moiety has been conveniently functionalized with dithiocarbamate giving rise to a ditopic ligand, which, once coordinated to the metal ion, is expected to prevent the coordination of the metal to the sulfur atoms of cytoplasmic proteins. The X-ray crystal structures as well as the DFT studies performed herein show that L^{2-} is a versatile, flexible platform, which can be easily adapted to different environments since the distance between the platinum ions can be varied, thus providing a variety of conformations when interacting with DNA. The 2-fold positive charge undoubtedly favors the affinity of the metal complexes with anionic species, such as anionic proteins present in the cell membrane as well as the polyanionic phosphate backbone of DNA, facilitating both the cellular uptake and DNA interaction. Further studies in order to clarify all these aspects are in progress.

■ ASSOCIATED CONTENT

SI Supporting Information

The Supporting Information is available free of charge at <https://pubs.acs.org/doi/10.1021/acs.inorgchem.0c02068>.

IR, ^1H , ^{13}C , and ^{31}P NMR spectra for **1–5**, ^{11}B NMR spectra for **3** and **4**, HR-ESI⁺ mass spectra for compounds **1**, **2**, and **5**, optimized geometry of conformer **1a**, selected calculated bond distances and angles of the optimized geometries, and optimized Cartesian coordinates obtained with DFT calculations (PDF)

Accession Codes

CCDC 2014769–2014772 contain the supplementary crystallographic data for this paper. These data can be obtained free of charge via www.ccdc.cam.ac.uk/data_request/cif, or by emailing data_request@ccdc.cam.ac.uk, or by contacting The Cambridge Crystallographic Data Centre, 12 Union Road, Cambridge CB2 1EZ, UK; fax: +44 1223 336033.

■ AUTHOR INFORMATION

Corresponding Authors

Teresa Rodríguez-Blas – Grupo METMED, Departamento de Química & Centro de Investigaciones Científicas Avanzadas (CICA), Universidade da Coruña, 15071 A Coruña, Spain; orcid.org/0000-0001-5078-1093; Email: teresa.rodriguez.blas@udc.es

Victor Barba – Centro de Investigaciones Químicas-IICBA, Universidad Autónoma del Estado de Morelos, 62209 Cuernavaca, Morelos, Mexico; Email: vbarba@uaem.mx

Authors

Antonino Arenaza-Corona – Grupo METMED, Departamento de Química & Centro de Investigaciones Científicas Avanzadas (CICA), Universidade da Coruña, 15071 A Coruña, Spain; Centro de Investigaciones Químicas-IICBA, Universidad Autónoma del Estado de Morelos, 62209 Cuernavaca, Morelos, Mexico

M. Delfina Couce-Fortúnez – Departamento de Química Inorgánica, Instituto de Investigación Sanitaria Galicia Sur, Facultade de Química, Universidad de Vigo, 36310 Vigo, Spain

Andrés de Blas – Grupo METMED, Departamento de Química & Centro de Investigaciones Científicas Avanzadas (CICA), Universidade da Coruña, 15071 A Coruña, Spain; orcid.org/0000-0001-8548-9658

David Morales-Morales – Instituto de Química, Universidad Nacional Autónoma de México, 04510 Ciudad de México, Mexico; orcid.org/0000-0002-7984-1819

Rosa Santillan – Departamento de Química, Centro de Investigación y de Estudios Avanzados del IPN, 07000 Ciudad de México, Mexico

Herbert Höpfl – Centro de Investigaciones Químicas-IICBA, Universidad Autónoma del Estado de Morelos, 62209 Cuernavaca, Morelos, Mexico; orcid.org/0000-0002-4027-0131

Complete contact information is available at:

<https://pubs.acs.org/10.1021/acs.inorgchem.0c02068>

Author Contributions

The manuscript was written through contributions of all authors. All authors have given approval to the final version of the manuscript.

Notes

The authors declare no competing financial interest.

■ ACKNOWLEDGMENTS

A.A.-C. and V.B. thank Consejo Nacional de Ciencia y Tecnología (CONACyT) of México for generous financial support (Project 33602). A.A.-C., V. B., and H.H. thank the Laboratorio Nacional de Estructura de Macromoléculas (CONACYT 294406) for the NMR and mass data. D.M.-M. would like to thank PAPIIT-DGAPA-UNAM (PAPIIT IN210520) and CONACyT A1-S-33933 for generous financial support. T.R.-B. and A.d.B. are grateful to Ministerio de Economía y Competitividad (CTQ2016-74862P) and Universidade da Coruña in Spain for financial support. The authors are indebted to Centro de Supercomputación de Galicia (CESGA) for providing the computer facilities. We also appreciate the help of Dr. G. Mengod (CSIC-IDIBAPS of Barcelona, Spain) for providing the human cervix carcinoma cell line HeLa-229 and of Dr. A. Lamas (Unidade de Raios X RIAIDT at University of Santiago de Compostela, Spain) for useful crystallographic discussions.

■ REFERENCES

- (1) Key Facts on Cancer, World Health Organization (WHO). <http://www.who.int/news-room/fact-sheets/detail/cancer> (accessed 2020-06-01).
- (2) Rozenzweig, M.; Von Hoff, D. D.; Slavik, M.; Muggia, F. M. Cis-diamminedichloroplatinum(II). A new anticancer drug. *Ann. Intern. Med.* **1977**, *86*, 803–812.
- (3) Giaccone, G. Clinical Perspectives on Platinum Resistance. *Drugs* **2000**, *59*, 9–17.
- (4) Kelland, L. The resurgence of platinum-based cancer chemotherapy. *Nat. Rev. Cancer* **2007**, *7*, 573–584.
- (5) Fichtinger-Schepman, A. M.; van der Veer, J. L.; den Hartog, J. H.; Lohman, P. H.; Reedijk, J. Adducts of the antitumor drug cis-diamminedichloroplatinum(II) with DNA: formation, identification, and quantitation. *Biochemistry* **1985**, *24*, 707–713.
- (6) Temple, M. D.; McFadyen, W. D.; Holmes, R. J.; Denny, W. A.; Murray, V. Interaction of cisplatin and DNA-targeted 9-aminoacridine platinum complexes with DNA. *Biochemistry* **2000**, *39*, 5593–5599.
- (7) Wilson, J. J.; Lippard, S. J. Synthetic methods for the preparation of platinum anticancer complexes. *Chem. Rev.* **2014**, *114*, 4470–4495.
- (8) Galluzzi, L.; Senovilla, L.; Vitale, I.; Michels, J.; Martins, I.; Kepp, O.; Castedo, M.; Kroemer, G. Molecular mechanisms of cisplatin resistance. *Oncogene* **2012**, *31*, 1869–1883.
- (9) Shen, D.-W.; Pouliot, L. M.; Hall, M. D.; Gottesman, M. M. Cisplatin resistance: Acellular self-defense mechanism resulting from

multiple epigenetic and genetic changes. *Pharmacol. Rev.* **2012**, *64*, 706–721.

(10) Cvitkovic, E. Cumulative toxicities from cisplatin therapy and current cytoprotective measures. *Cancer Treat. Rev.* **1998**, *24*, 265–281.

(11) Screnci, D.; McKeage, M. J. Platinum neurotoxicity: clinical profiles, experimental models and neuroprotective approaches. *J. Inorg. Biochem.* **1999**, *77*, 105–110.

(12) Jadon, A. S.; Bhadauriya, P.; Sharma, M. An Integrative review of cisplatin: the first metal anti-tumor drug. *Journal of Drug Delivery & Therapeutics* **2019**, *9*, 673–677.

(13) Daugaard, G.; Abildgaard, U. Cisplatin nephrotoxicity. A review. *Cancer Chemother. Pharmacol.* **1989**, *25*, 1–9.

(14) Pabla, N.; Dong, Z. Cisplatin nephrotoxicity: mechanisms and renoprotective strategies. *Kidney Int.* **2008**, *73*, 994–1007.

(15) Ali, I.; Wani, W. A.; Saleem, K.; Haque, A. Platinum compounds: A hope for future cancer chemotherapy. *Anti-Cancer Agents Med. Chem.* **2013**, *13*, 296–306.

(16) Medici, S.; Peana, M.; Nurchi, V. M.; Lachowicz, J. I.; Crisponi, G.; Zoroddu, M. A. Noble metals in medicine: latest advances. *Coord. Chem. Rev.* **2015**, *284*, 329–350.

(17) Hogarth, G. Metal-dithiocarbamate complexes: chemistry and biological activity. *Mini-Rev. Med. Chem.* **2012**, *12*, 1202–1215.

(18) Ronconi, L.; Fregona, D. The Midas touch in cancer chemotherapy: from platinum- to gold-dithiocarbamate complexes. *Dalton Trans.* **2009**, 10670–10680.

(19) (a) Marzano, C.; Fregona, D.; Baccichetti, F.; Trevisan, A.; Giovagnini, L.; Bordin, F. Citotoxicity and DNA damage induced by a new platinum(II) complex with pyridine and dithiocarbamate. *Chem.-Biol. Interact.* **2002**, *140*, 215–229. (b) Marzano, C.; Trevisan, A.; Giovagnini, L.; Fregona, D. Synthesis of a new platinum(II) complex: anticancer activity and nephrotoxicity in vitro. *Toxicol. In Vitro* **2002**, *16*, 413–419.

(20) Kralj, M.; Tušek-Božić, L.; Frkanec, L. Biomedical potentials of crown ethers: prospective antitumor agents. *ChemMedChem* **2008**, *3*, 1478–1492.

(21) McPhee, M. M.; Kern, J. T.; Hoster, B. C.; Kerwin, S. M. Propargylic sulfone-armed lariat crown ethers: alkali metal ion-regulated DNA cleavage agents. *Bioorg. Chem.* **2000**, *28*, 98–118.

(22) Marjanović, M.; Kralj, M.; Supek, F.; Frkanec, L.; Piantanida, I.; Šmuc, T.; Tušek-Božić, L. Antitumor potential of crown ethers: structure-activity relationships, cell cycle disturbances and cell death studies of a series of ionophores. *J. Med. Chem.* **2007**, *50*, 1007–1018.

(23) Frühauf, S.; Zeller, W. J. New platinum, titanium and ruthenium complexes with different patterns of DNA damage in rat ovarian tumor cells. *Cancer Res.* **1991**, *51*, 2943–2948.

(24) Frühauf, S.; Zeller, W. J. In vitro evaluation of platinum, titanium and ruthenium metal complexes in cisplatin-sensitive and -resistant rat ovarian tumors. *Cancer Chemother. Pharmacol.* **1991**, *27*, 301–307.

(25) Gund, A.; Keppler, B. K. Structure of an antineoplastic platinum complex with a bipyridyl-crown ether. *Angew. Chem., Int. Ed. Engl.* **1994**, *33*, 186–188.

(26) Yoo, J. S.; Sohn, Y. S.; Do, Y. K. Synthesis, structures and antitumor activity of the first crown ester-linked bipyridyl platinum complexes. *J. Inorg. Biochem.* **1999**, *73*, 187–193.

(27) Jansen, B. A. J.; Wielaard, P.; den Dulk, H.; Brouwer, J.; Reedijk, J. Oxa-aza crown ethers as ligands for mixed-ligand cisplatin derivatives and dinuclear platinum anticancer drugs. *Eur. J. Inorg. Chem.* **2002**, *2002*, 2375–2379.

(28) Keller, H. J.; Keppler, B. Antineoplastic active platinum-crown ether complexes and a pharmaceutical containing them. WO8503078A1, 1985.

(29) Celis, N. A.; Villamil-Ramos, R.; Höpfl, H.; Hernandez-Ahuactzi, I. F.; Sanchez, M.; Zamudio-Rivera, L. S.; Barba, V. Dinuclear monomeric and macrocyclic organotin dithiocarbamates derived from 1,10-diaza-18-crown-6 and 4,4'-trimethylenedipiperidine. *Eur. J. Inorg. Chem.* **2013**, *2013*, 2912–2922.

(30) Toscani, A.; Heliövaara, E. K.; Hena, J. B.; White, A. J. P.; Wilton-Ely, J. D. E. T. Multimetallic alkenyl complexes bearing macrocyclic dithiocarbamate ligands. *Organometallics* **2015**, *34*, 494–505.

(31) Arias, J.; Bardají, M.; Espinet, P. Mononuclear, dinuclear, and hexanuclear gold(I) complexes with (aza-15-crown-5)dithiocarbamate. *Inorg. Chem.* **2008**, *47*, 1597–606.

(32) Patel, G.; Kumar, A.; Pal, U.; Menon, S. Potassium ion recognition by facile dithiocarbamate assembly of benzo-15-crown-5-gold nanoparticles. *Chem. Commun.* **2009**, 1849–1851.

(33) Berry, N. G.; Shimell, T. W.; Beer, P. D. Heteroditopic transition metal dithiocarbamate receptors for binding cation-anion ion pairs. *J. Supramol. Chem.* **2002**, *2*, 89–92.

(34) Tzeng, B.-C.; Chao, A. Single-crystal-to-single-crystal transformation and solvochromic luminescence of a dinuclear gold(I)-(aza-[18]crown-6)dithiocarbamate compound. *Chem. - Eur. J.* **2015**, *21*, 2083–2089.

(35) Mehta, V. N.; Solanki, J. N.; Kailasa, S. K. Selective visual detection of Pb(II) ion via gold nanoparticles coated with a dithiocarbamate-modified 4'-aminobenzo-18-crown-6. *Microchim. Acta* **2014**, *181*, 1905–1915.

(36) Liu, S.; He, Z. Crowned dithiocarbamate metal complexes and methods for their use. WO2005077962A3, 2005.

(37) Arenaza-Corona, A.; Villamil-Ramos, R.; Guerrero-Álvarez, J.; Höpfl, H.; Barba, V. Bis-dithiocarbamates derived from 1,10-diaza-18-crown-6 as ligand tectons for 1D, 2D and 3D supramolecular structure arrangements. *CrystEngComm* **2020**, *22*, 1063–1077.

(38) Agilent Technologies, *CrysAlisPro*, Version 1.171.37.35; Yarnton, O., United Kingdom, 2014.

(39) Dolomanov, O. V.; Bourhis, L. J.; Gildea, R. J.; Howard, J. A. K.; Puschmann, H. OLEX2: a complete structure solution, refinement and analysis program. *J. Appl. Crystallogr.* **2009**, *42*, 339–341.

(40) Sheldrick, G. M. Crystal Structure Refinement with SHELXL. *Acta Crystallogr., Sect. C: Struct. Chem.* **2015**, *C71*, 3–8.

(41) Rees, B.; Jenner, L.; Yusupov, M. Bulk-solvent correction in large macromolecular structures. *Acta Crystallogr., Sect. D: Biol. Crystallogr.* **2005**, *D61*, 1299–1301.

(42) Macrae, C. F.; Edgington, P. R.; McCabe, P.; Pidcock, E.; Shields, G. P.; Taylor, R.; Towler, M.; van de Streek, J. Mercury: visualization and analysis of crystal structures. *J. Appl. Crystallogr.* **2006**, *39*, 453–457.

(43) Frisch, M. J.; Trucks, G. W.; Schlegel, H. B.; Scuseria, G. E.; Robb, M. A.; Cheeseman, J. R.; Scalmani, G.; Barone, V.; Petersson, G. A.; Nakatsuji, H.; Li, X.; Caricato, M.; Marenich, A. V.; Bloino, J.; Janesko, B. G.; Gomperts, R.; Mennucci, B.; Hratchian, H. P.; Ortiz, J. V.; Izmaylov, A. F.; Sonnenberg, J. L.; Williams-Young, D.; Ding, F.; Lipparini, F.; Egidi, F.; Goings, J.; Peng, B.; Petrone, A.; Henderson, T.; Ranasinghe, D.; Zakrzewski, V. G.; Gao, J.; Rega, N.; Zheng, G.; Liang, W.; Hada, M.; Ehara, M.; Toyota, K.; Fukuda, R.; Hasegawa, J.; Ishida, M.; Nakajima, T.; Honda, Y.; Kitao, O.; Nakai, H.; Vreven, T.; Throssell, K.; Montgomery, J. A., Jr.; Peralta, J. E.; Ogliaro, F.; Bearpark, M. J.; Heyd, J. J.; Brothers, E. N.; Kudin, K. N.; Staroverov, V. N.; Keith, T. A.; Kobayashi, R.; Normand, J.; Raghavachari, K.; Rendell, A. P.; Burant, J. C.; Iyengar, S. S.; Tomasi, J.; Cossi, M.; Millam, J. M.; Klene, M.; Adamo, C.; Cammi, R.; Ochterski, J. W.; Martin, R. L.; Morokuma, K.; Farkas, O.; Foresman, J. B.; Fox, D. J. *Gaussian 16*, Revision C.01; Gaussian Inc.: Wallingford, CT, 2019.

(44) Austin, A.; Petersson, G.; Frisch, M. J.; Dobek, F. J.; Scalmani, G.; Throssell, K. A density functional with spherical atom dispersion terms. *J. Chem. Theory Comput.* **2012**, *8*, 4989–5007.

(45) (a) Fuentealba, P.; Preuss, H.; Stoll, H.; Von Szentpály, L. A Proper account of core-polarization with pseudopotentials – Single valence-electron alkali compounds. *Chem. Phys. Lett.* **1982**, *89*, 418–422. (b) Fuentealba, P.; Stoll, H.; Von Szentpály, L.; Schwerdtfeger, P.; Preuss, H. On the reliability of semi-empirical pseudopotentials – simulation of Hartree-Fock and Dirac-Fock results. *J. Phys. B: At. Mol. Phys.* **1983**, *16*, L323–L328. (c) Wedig, U.; Dolg, M.; Stoll, H.; Preuss, H. Energy-adjusted Pseudopotentials for Transition-Metal Elements. In *Quantum Chemistry: The Challenge of Transition Metals and Coordination Chemistry*; Veillard, A., Ed; NATO ASI Series C no 176; Reidel: Dordrecht, 1986; pp 79–89. (d) Andrae, D.; Haeussermann, U.; Dolg, M.; Stoll, H.; Preuss, H. Energy-adjusted ab

initio pseudopotentials for the 2nd and 3rd row transition-elements. *Theor. Chem. Acc.* **1990**, *77*, 123–41.

(46) Scalmani, G.; Frisch, M. J. Continuous surface charge polarizable continuum models of solvation. I. General formalism. *J. Chem. Phys.* **2010**, *132*, 114110.

(47) Lukyanenko, N. G.; Bogatsky, A. V.; Kirichenko, T. I.; Scherbakov, S. V.; Nazarova, N. Y. Macroheterocycles; XX. Synthesis of cryppands containing urea and thiourea moieties. *Synthesis* **1984**, *1984*, 137.

(48) Chan, L. T.; Chen, H. W.; Fackler, J. P.; Masters, A. F.; Pan, W. H. Sulfur chelates. 38. Preparations and x-ray structure determinations of $M(S_2CNEt_2)(PR_3)Cl$ ($M = Ni, R = Et; M = Pd, Pt, R = C_6H_5$). *Inorg. Chem.* **1982**, *21*, 4291–4295.

(49) Pastorek, R.; Kameníček, J.; Trávníček, Z.; Husárek, J.; Duffy, N. Benzylisopropylidithiocarbamate complexes of nickel with triphenylphosphine in the coordination sphere. *Polyhedron* **1999**, *18*, 2879–2883.

(50) Pastorek, R.; Kameníček, J.; Cvek, B.; Pavlíček, M.; Sindelar, Z.; Zak, Z. Nickel(II) di(pentyl)dithiocarbamates with P ligands. *J. Coord. Chem.* **2003**, *56*, 1123–1129.

(51) Pastorek, R.; Kameníček, J.; Husárek, J.; Slovák, V.; Pavlíček, M. Ni(II) benzylbutylidithiocarbamates containing monodentate phosphines. *J. Coord. Chem.* **2007**, *60*, 485–494.

(52) Pastorek, R.; Štarha, P.; Drahoš, B.; Trávníček, Z. Effect of diverse solvents on the composition and structure of mixed-ligand nickel(II) dithiocarbamates: $[NiX(ndtc)(PPh_3)]$. *Polyhedron* **2014**, *69*, 174–180.

(53) Román, P.; Baitia, J. I.; Luque, A.; Guzmán-Miralles, C. Synthesis, chemical characterization, structural data and thermal behaviour of 3-methylpyridinium salts of 1,2-dithiooxalato-*s,s'* complexes with formula $(HB)_2[M(S_2C_2O_2)_2]$ ($M = Ni^{II}, Pd^{II}$ and Pt^{II}). *Polyhedron* **1994**, *13*, 2311–2317.

(54) Guney, E.; Yilmaz, V. T.; Buyukgungor, O. Neutral and cationic palladium(II) and platinum(II) complexes of 2,2'-dipyridylamine with saccharinate: Syntheses, spectroscopic, structural, fluorescent and thermal studies. *Inorg. Chim. Acta* **2010**, *363*, 2416–2424.

(55) Khan, H.; Badshah, A.; Said, M.; Murtaza, G.; Ahmad, J.; Jean-Claude, B. J.; Todorova, M.; Butler, I. S. Anticancer metal-olopharmaceutical agents based on mixed-ligand palladium(II) complexes with dithiocarbamates and tertiary organophosphine ligands. *Appl. Organomet. Chem.* **2013**, *27*, 387–395.

(56) Arenaza-Corona, A.; Morales-Morales, D.; Hernández-Ahuactzi, I. F.; Barba, V. Structural and conformational changes in $[M(1,10-diaza-18-crown-6)Cl_2]$ ($M = Pd, Pb$) complexes: a crystallographic and theoretical study. *CrystEngComm* **2018**, *20*, 6733–6740.

(57) Steed, J. W. First- and second-sphere coordination chemistry of alkaline metal crown ether complexes. *Coord. Chem. Rev.* **2001**, *215*, 171–221.

(58) Batsanov, S. S. Van der Waals Radii of Elements. *Inorg. Mater.* **2001**, *37*, 871–885.

(59) Roy, S.; Puddephatt, R. J.; Scott, J. D. Mechanism and energetics of reductive elimination of ethane from some tetramethylplatinum(IV) complexes. *J. Chem. Soc., Dalton Trans.* **1989**, 2121–2125.

(60) Perez, J. M.; Montero, E. I.; Quiroga, A. G.; Fuertes, M. A.; Alonso, C.; Navarro-Ranninger, C. Cellular uptake, DNA binding and apoptosis induction of cytotoxic $trans-[PtCl_2(N,N-dimethylamine)(isopropylamine)]$ in A2780cisR ovarian tumor cells. *Metal Based Drugs* **2001**, *8*, 29–37.

(61) Perez, J. M.; Kelland, L. R.; Montero, E. I.; Boxall, F. E.; Fuertes, M. A.; Alonso, C.; Navarro-Ranninger, C. Antitumor and cellular pharmacological properties of a novel platinum(IV) complex: $trans-[PtCl_2(OH)_2(dimethylamine)(isopropylamine)]$. *Mol. Pharmacol.* **2003**, *63*, 933–944.

(62) Kelland, L. R.; Barnard, C. F. J.; Mellish, K. J.; Jones, M.; Goddard, P. M.; Valenti, M.; Bryant, A.; Murrer, B. A.; Harrap, K. R. A novel *trans*-platinum coordination complex possessing *in vitro* and *in vivo* antitumor activity. *Cancer Res.* **1994**, *54*, 5618–5622.

(63) Yilmaz, V. T.; Icel, C.; Aygun, M.; Erkisa, M.; Ulukaya, E. Pd(II) and Pt(II) saccharinate complexes of bis(diphenylphosphino)-

propane/butane: synthesis, structures, antiproliferative activity and mechanism of action. *Eur. J. Med. Chem.* **2018**, *158*, 534–547.

(64) Politzer, P.; Laurence, P. R.; Jayasuriya, K. Molecular electrostatic potentials: an effective tool for the elucidation of biochemical phenomena. *Environ. Health Perspect.* **1985**, *61*, 191–202.